

ARTICLE

Delta-secretase (AEP) mediates tau-splicing imbalance and accelerates cognitive decline in tauopathies

Zhi-Hao Wang^{1,2} , Pai Liu², Xia Liu², Shan Ping Yu³, Jian-Zhi Wang^{1,4}, and Keqiang Ye^{2,5} 

SRPK2 is abnormally activated in tauopathies including Alzheimer’s disease (AD). SRPK2 is known to play an important role in pre-mRNA splicing by phosphorylating SR-splicing factors. Dysregulation of tau exon 10 pre-mRNA splicing causes pathological imbalances in 3R- and 4R-tau, leading to neurodegeneration; however, the role of SRPK2 in these processes remains unclear. Here we show that delta-secretase (also known as asparagine endopeptidase; AEP), which is activated in AD, cleaves SRPK2 and increases its nuclear translocation as well as kinase activity, augmenting exon 10 inclusion. Conversely, AEP-uncleavable SRPK2 N342A mutant increases exon 10 exclusion. Lentiviral expression of truncated SRPK2 increases 4R-tau isoforms and accelerates cognitive decline in htau mice. Uncleavable SRPK2 N342A expression improves synaptic functions and prevents spatial memory deficits in tau intronic mutant FTDP-17 transgenic mice. Hence, AEP mediates tau-splicing imbalance in tauopathies via cleaving SRPK2.

Introduction

Alzheimer’s disease (AD) is a progressive neurodegenerative disorder with gradual cognitive function decline. The neuropathology of AD is characterized by both the accumulation of toxic, extracellular senile plaques with amyloid- β (A β) as a major component and neurofibrillary tangles (NFTs) resulting from the aggregation of hyperphosphorylated and truncated tau. The conformational changed tau alters the protein structures and forms paired helical filaments and NFTs, which are characterized in a wide range of neurodegenerative diseases, collectively called as tauopathies, including AD, frontotemporal dementia with parkinsonism-17 (FTDP-17), Pick disease (PiD), etc. (Wang and Mandelkow, 2016). Recently, we have reported that asparagine endopeptidase (AEP) is an age-dependent cysteine protease that is highly activated in AD patients and cleaves tau at both N255 and N368 residues in the brains and promotes its aggregation and neurotoxicities. Blockade of tau fragmentation by AEP prevents tau P301S mutant to trigger synaptic dysfunctions and cognitive deficits (Zhang et al., 2014). In addition, AEP also acts as delta-secretase by shredding amyloid precursor protein (APP) on N373 and N585 residues, generating C-terminal APP (aa 586–695) truncation that is a much more efficient substrate for BACE1 to produce A β than full-length (FL) APP. Consequently, inhibition

of AEP cleavage of APP decreases A β production and diminishes senile plaque deposit, rescuing the learning and memory deficits (Zhang et al., 2015). Accordingly, inhibition of AEP by small molecular inhibitors in various AD mouse models abrogates AD pathologies, exerting the prominent therapeutic efficacy (Zhang et al., 2016, 2017b).

Serine-arginine protein kinase 2 (SRPK2) is a member of SRPKs, a group of cell cycle-regulated serine kinases. SRPKs recognize and phosphorylate protein substrates with serine-arginine dipeptide repeats (Gui et al., 1994). They are mainly involved in regulating pre-mRNA splicing via phosphorylating splicing factors, such as alternative splicing factor/splicing factor 2 (ASF/SF2) and SC35 (Ding et al., 2006). SRPKs also regulate the subcellular localization of splicing factors ASF/SF2 through phosphorylation (Koizumi et al., 1999). Unlike the ubiquitously expressed SRPK1, SRPK2 is highly enriched in the brain and plays an important role in controlling neuronal functions. Our previous study supports that SRPK2 participates in the neuronal survival, cell cycle progression, and memory determination in AD (Chan and Ye, 2013). For instance, we have shown that SRPK2 mediates cell cycle progression and cell death in mature neurons (Jang et al., 2008, 2009). Moreover, we found that SRPK2 is a caspase sub-

¹Department of Pathophysiology, Key Laboratory of Ministry of Education of Neurological Diseases, Tongji Medical College, Huazhong University of Science and Technology, Wuhan, China; ²Department of Pathology and Laboratory Medicine, Emory University School of Medicine, Atlanta, GA; ³Department of Anesthesiology, Emory University School of Medicine, Atlanta, GA; ⁴Co-innovation Center of Neuroregeneration, Nantong University, Nantong, China; ⁵Tongji Hospital, Tongji University School of Medicine, Shanghai, China.

Correspondence to Keqiang Ye: kye@emory.edu; Jian-Zhi Wang: wangjz@mails.tjmu.edu.cn.

© 2018 Wang et al. This article is distributed under the terms of an Attribution–Noncommercial–Share Alike–No Mirror Sites license for the first six months after the publication date (see <http://www.rupress.org/terms/>). After six months it is available under a Creative Commons License (Attribution–Noncommercial–Share Alike 4.0 International license, as described at <https://creativecommons.org/licenses/by-nc-sa/4.0/>).

strate, which promotes neuronal apoptosis after caspase cleavage (Hong et al., 2011). Furthermore, we demonstrated that the activity of SRPK2 is focally enhanced in both human and rodent brains of AD. SRPK2 phosphorylates tau on S214 and suppresses microtubule (MT) polymerization. Depleting SRPK2 in the hippocampus alleviates the memory defect and improves the induction of long-term potentiation (LTP) in APP/PS1 mice. Hence, these findings suggest that SRPK2 is implicated in the pathogenesis of AD (Hong et al., 2012). Most recently, we showed that SRPK2 phosphorylates AEP on S226 residue and enhances its protease activity, facilitating AD pathogenesis (Wang et al., 2017).

Tau is a MT-associated protein enriched in axons of neurons and plays a crucial role in various neuronal functions by assembling and stabilizing MTs. Human *MAPT* gene encoding tau protein consists of 16 exons. Alternative splicing of exons 2, 3, and 10 generates six different isoforms in adult brain. Exon 10 encodes the second of four MT-binding repeat domains, and its alternative splicing produces tau isoforms with three or four MT-binding repeats, named 3R-tau or 4R-tau, that are under developmental and cell type-specific regulation (Goedert et al., 1989). Interestingly, only 3R is selectively expressed in the developing brain, whereas approximately equal levels of 3R-tau and 4R-tau are expressed in normal adult human brain (Goedert et al., 1989; Andreadis, 2005). Unbalanced ratios of 3R-tau/4R-tau trigger neurodegeneration in FTDP-17 and other neurodegenerative disorders, including PiD, corticobasal degeneration, and progressive supranuclear palsy (PSP; Neumann et al., 2001; Bronner et al., 2005; Yoshida, 2006). To date, >50 disease-associated mutations have been identified in *MAPT*, with one third of them affecting E10 splicing (Ghetti et al., 2015). Mutations in tau gene (*MAPT*) have been discovered and directly linked tau abnormalities to neurodegenerative diseases (Hutton et al., 1998; Spillantini et al., 1998), though there are no known tau mutations that have occurred in AD. In AD, there is a disproportionate level of the 3R-tau isoform compared with the 4R form, and this could be a key factor driving the formation of tau into paired helical filaments (Goedert and Jakes, 2005; Espinoza et al., 2008). In the current study, we report that AEP cleaves SRPK2 in human AD brains and escalates its kinase activity. The active SRPK2 phosphorylates serine/arginine (SR) proteins including SC35 and ASF/SF2-splicing factors, mediating tau exon 10 splicing and tilting the balance between 3R-tau and 4R-tau. Overexpressing AEP-truncated SRPK2 fragments in 3R-enriched WT htau mice (*MAPT* mice) elevates 4R-tau, accelerating tau pathology and cognitive dysfunctions, whereas overexpressing AEP-uncleavable SRPK2 N342A mutant in 4R abundant tau intronic mutant (10 +16C → T) FTDP-17 mouse model (tau609 mice) augments 3R-tau, decreasing tau pathology and cognitive deficits.

Results

AEP cleaves SRPK2 at N342 residue

Most recently, we reported that SRPK2 phosphorylates human AEP on S226 and enhances its auto-cleavage and enzymatic activities in AD (Wang et al., 2017). Proteomic analysis of *Igmn* WT and knockout brains indicates that SRPK2 might be a potential target of AEP. To explore whether AEP indeed cleaves SRPK2, we

performed an in vitro cleavage assay using *Igmn*^{+/+} and *Igmn*^{-/-} kidney lysates in the presence of purified recombinant glutathione S-transferase (GST)-SRPK2. Immunoblotting analysis showed that SRPK2 was selectively cut in WT, but not AEP-null lysates under pH 6.0, whereas it remained intact under neutral pH (Fig. 1 A). To examine whether the fragmentation was executed by AEP in the lysates, we conducted truncation assay with AEP enzymatic-dead (C189S) or uncleavable inactive N323A mutant. Although WT AEP robustly cut SRPK2, both inactive mutants failed in the cotransfected HEK293 cells (Fig. 1 B), indicating that AEP may mediate SRPK2 fragmentation. Moreover, titration assay with anti-AEP revealed that AEP antibody dose-dependently antagonized SRPK2 fragmentation, whereas anti-mouse IgG control was unable (Fig. 1 C), suggesting that the active AEP in the acidic lysates might be responsible for SRPK2 fragmentation. Consequently, the peptidic inhibitor AENK but not inactive control AEQK for AEP selectively blocked SRPK2 proteolytic cleavage (Fig. S1 A). Further, we observed the similar cleavage activity in *Igmn*^{+/+} but not *Igmn*^{-/-} brain lysates under pH 6.0 with endogenous SRPK2. Notably, the 50-kD band was the major product identified in the brain, suggesting that it is the dominant form of truncated SRPK2 in the brain (Fig. 1 D). Using purified SRPK2 recombinant protein and active AEP, we found that active AEP directly shredded SRPK2 into numerous fragments, supporting that AEP directly cleaves SRPK2 (Fig. S1 B). Liquid chromatography with tandem mass spectrometry analysis showed that N342 residue was the major cutting site on SRPK2 by AEP (Fig. S1 C). Site-directed mutagenesis demonstrated that N219, N342, and N435 were the potential cleaving residues on SRPK2 by AEP. Since N342A mutation completely blocked the main truncated band from SRPK2, thus N342 might be the predominant cutting site (Fig. 1 E). Interestingly, SRPK2-phosphorylated AEP (S226D) displayed a much stronger protease activity in cleaving SRPK2 than WT AEP, whereas unphosphorylated mutant S226A barely cut SRPK2 (Fig. S1 D), in alignment with our recent finding that SRPK2 phosphorylation of AEP escalates its protease activity (Wang et al., 2017).

To interrogate the cleavage activity on SRPK2, we generated rabbit polyclonal SRPK2 N342 and C343 antibodies. The antigen affinity column-purified antibody specifically recognized the truncated SRPK2, but not SRPK2 FL in primary neuronal cultures treated with A β 42, and the signal was totally stripped away by the preincubation with the free antigen (Fig. S2 A). This indicates that anti-SRPK2 N342 and C343 are very specific toward the truncated products. Noticeably, both N342 and C343 antibodies specifically recognized the truncated SRPK2 by AEP, and they were inactive when AEP was knocked out (Fig. S2, B and C), underscoring that these two antibodies selectively detect SRPK2 fragments truncated at N342 residue by AEP. The specificity of anti-SRPK2 antibodies (N342 and C343) was further validated with SRPK2 knockdown or overexpression (Fig. S2, D-F).

AEP cuts SRPK2 in human tauopathy brains

Our recent study shows that AEP is up-regulated and active in the brain in an age-dependent manner (Zhang et al., 2014, 2015, 2017a). As expected, we found that SRPK2 was gradually truncated in mouse brain during aging. Accordingly, SRPK2 N342

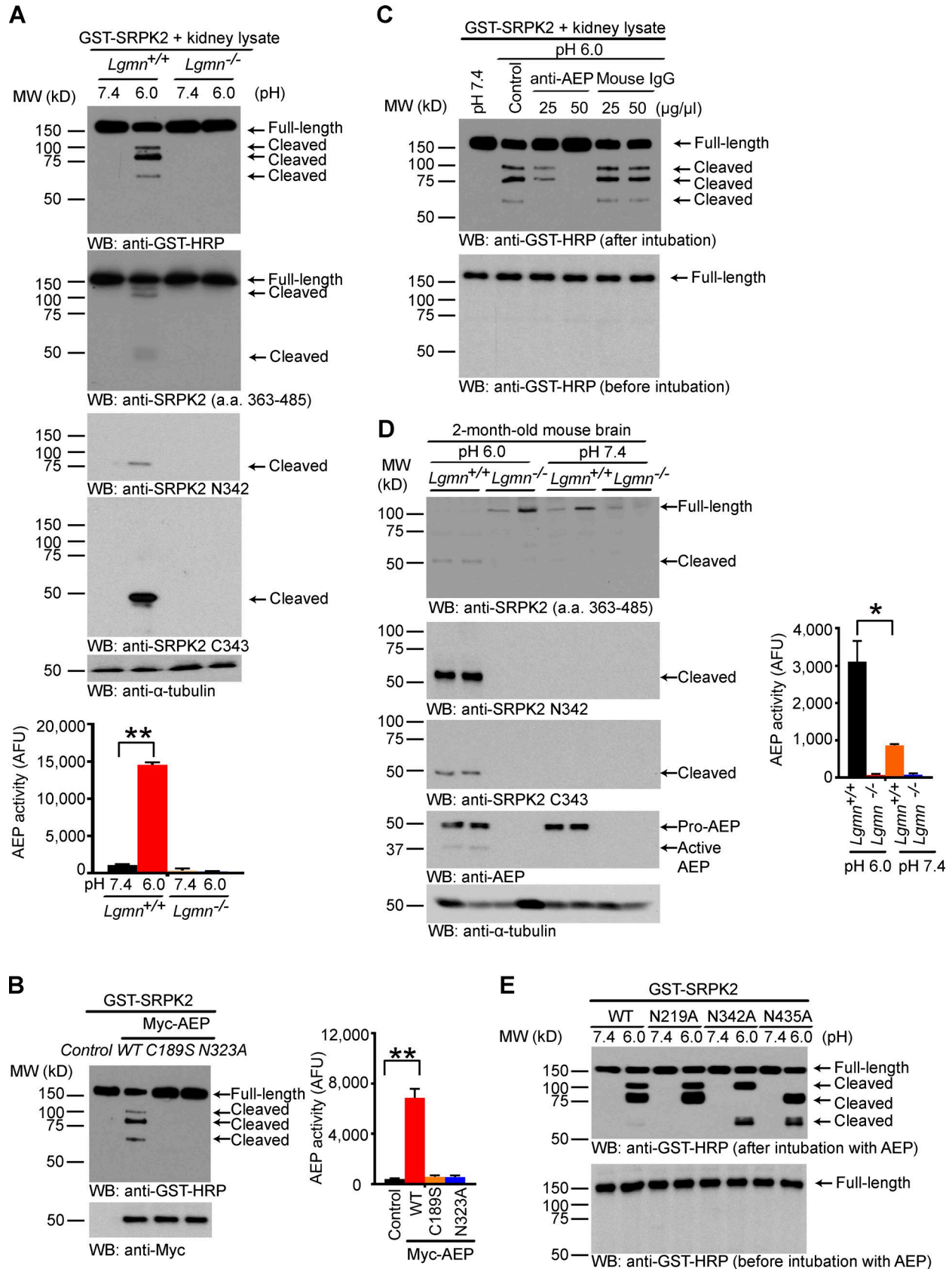


Figure 1. **AEP cleaves SRPK2.** (A) SRPK2 cleavage assay. Western blot showing the cleavage of GST-SRPK2 after transfected HEK293 cell lysates were incubated with kidney lysates from *Lgmn*^{+/+} or *Lgmn*^{-/-} mice at pH 7.4 or pH 6.0. Bar graph shows data as mean \pm SEM; $n = 3$ independent experiments; **, $P < 0.01$; one-way ANOVA. (B) Western blot showing the cleavage of SRPK2 by WT and enzymatic-dead mutated AEP constructs. Bar graph shows data as mean \pm SEM; $n = 3$ independent experiments; **, $P < 0.01$; one-way ANOVA. (C) Antibody titration assay. Mouse IgG was used as negative control. AEP antibody

fragment temporally escalated in the mouse brains (Fig. 2 A, first and second panels from the top). Our previous finding showed that SRPK2 T492 phosphorylation was also age-dependently augmented; so was the kinase activity (Hong et al., 2012). Consequently, its biological substrate tau S214 phosphorylation increased in a similar manner (Fig. 2 A, third and fourth panels from the top). As positive control, both AEP auto-cleavage and its well-characterized substrate tau N368 were elevated with the age increase (Fig. 2 A, seventh and eighth panels from the top). To examine whether AEP mediates SRPK2 fragmentation in AD mouse model, we knocked out *Lgmn* from 5XFAD mice and found that SRPK2 N342 was selectively cleaved in 5XFAD mice, and the cleavage was abrogated when AEP was depleted (Fig. 2 B, first and second panels from the top). Again, tau N368 was robustly truncated in 5XFAD but not 5XFAD/AEP^{-/-} mice (Fig. 2 B, seventh and eighth panels from the top). Once more, SRPK2 was strongly phosphorylated on T492 and activated in AD mouse model with 5XFAD stronger than 5XFAD/AEP^{-/-} mice. Consequently, tau S214 and acinus S422, another SR-enriched SRPK2 substrate that we identified previously (Jang et al., 2008), were potently phosphorylated by active SRPK2 (Fig. 2 B, third through sixth panels from the top). We made the similar observation in human AD brains, which exhibited prominent AEP, tau N368, and SRPK2 N342 cleavage. Again, p-SRPK2 T492, a marker for its kinase activation, tightly coupled with p-tau S214 in patient brains (Fig. 2 C). Collectively, these data strongly suggest that SRPK2 displays a much higher kinase activity in human AD brains, when it is cleaved by AEP.

To assess whether SRPK2 is also cleaved in other tauopathies, we performed immunoblotting with the brain samples from human FTDP-17 (tau P301L or G389R) and PSP patients and their age-matched controls. Evidence for the presence or absence of silver-positive neuronal tau inclusions was shown for AD, FTDP-17, and PSP brains as well as for the healthy control of similar age (Fig. S3 A). Notably, SRPK2 was prominently cut in both FTDP-17 and PSP patients, which was validated by both SRPK2 N342 and C343 antibodies (Fig. 2, D and E, first through fourth panels from the top). Surprisingly, SRPK2 was not cleaved in tau G389R mutant FTDP-17 patient (Fig. 2 D, last lane, first through fourth panels from the top). Strikingly, 3R-tau and 4R-tau appeared inversely correlated in these patient brains. SRPK2 truncation activities tightly linked to 4R-tau abundance in both tauopathies (Fig. 2, D and E, fourth through sixth panels from the top; Fig. S3, B and C), indicating that SRPK2 might implicate in tau exon 10 alternative splicing. Subcellular fractionation supported that truncated SRPK2 fragments were preferentially distributed in the nuclear fraction versus cytosolic fraction. Moreover, C-terminal SRPK2 fragment (C343–688) was allocated more in the nuclear than N-terminal fragment (1–342), but they barely resided in the lysosomal fraction (Fig. 2 F). Immunofluorescent staining showed that AEP was augmented in both FTDP-17 and PSP brains,

colocalizing with pronounced SRPK2 N342 or SRPK2 C343 fragment as compared with these of healthy controls (Fig. S3, D and E). Together, these findings support that AEP is activated in human patient brains with tauopathies and cleaves SRPK2 at N342, associating with augmented kinase activity.

AEP-cleaved SRPK2 displays higher kinase activity and translocates into the nucleus

SRPK2 contains bipartite kinase domains on both N and C termini with a cytoplasm tethering spacer between them (Ding et al., 2006). To further assess the biological consequence of AEP cleavage on SRPK2 kinase activity, we monitored tau S214 phosphorylation in the presence of SRPK2 FL and mixed fragments and purified recombinant GST-tau proteins. Using AEP WT and enzymatic-dead C189S, we found that AEP-cleaved SRPK2 possessed much higher kinase activity toward tau than uncleaved SRPK2. Quantitative analysis revealed that p-tau S214 was increased time-dependently with fragments much stronger than SRPK2 FL, indicating that AEP cleavage escalates SRPK2 kinase activity (Fig. S4, A and B). To determine which kinase domain possesses more robust enzymatic activity, we conducted an *in vitro* phosphorylation assay with purified fragments and SRPK2 FL in the presence of acinus and tau recombinant proteins, respectively. Immunoblotting revealed that both fragments exhibited more robust kinase activities than SRPK2 FL toward p-acinus S422 and p-tau S214 (Fig. 3 A). Immunofluorescent staining with GFP-SRPK2 constructs showed that WT SRPK2 has its two truncated fragments localized in both the cytoplasm and the nucleus, whereas uncleavable mutant N342A exclusively resided in the cytoplasm (Fig. 3 B), indicating that AEP cleavage is required for SRPK2 nuclear translocation. Infection of SRPK2 fragments in neurons significantly redistributed SC35 from the nuclear speckles into the nucleoplasm, whereas N342A failed (Fig. 3 C), confirming a previous report that SRPK2 disassembles the nuclear speckle (Kuroyanagi et al., 1998). Interestingly, the insoluble tau from tau P301S mouse brains elevated AEP expression in primary neurons, leading to the up-regulation of AEP, which subsequently truncated SRPK2 that was positive for N342 staining. The elevated N-terminal 1–342 fragment distributed in both the cytoplasm and the nucleus, whereas C-terminal SRPK2 (C343–688) predominantly resided in the nucleus, resulting in SC35 nuclear relocation (Fig. S4, C and D). Subcellular fractionation demonstrated that insoluble tau but not soluble tau fraction from tau P301S mouse brains provoked AEP activation in the cytosolic fraction, triggering SRPK2 cleavage. Fitting with immunofluorescent staining, C-terminal SRPK2 C343 fragment was relatively more abundant than N-terminal N342 fragment in the nuclear fraction in SH-SY5Y cells treated with insoluble tau. Noticeably, insoluble tau elevated 4R-tau and decreased 3R-tau in the cytosolic fraction of neuronal SH-SY5Y cells. It is worth noting that splicing factors ASF and SC35 expression levels were augmented in the nuclear

dose-dependently neutralized SRPK2 cleavage in the lysates. (D) Western blot showing the cleavage of endogenous SRPK2 by AEP. Bar graph shows data as mean \pm SEM; $n = 3$ independent experiments; *, $P < 0.05$; one-way ANOVA. (E) Cleavage of mutant SRPK2 by AEP. SRPK2 cleavage was analyzed by Western blot after lysates of HEK293 cell expressing GST-SRPK2 WT, N219A, N342A, or N435A mutants were incubated with active mouse kidney lysates. Western blot data in A–E are representative of three independent experiments. AFU, arbitrary fluorescence units; MW, molecular weight; WB, Western blot.

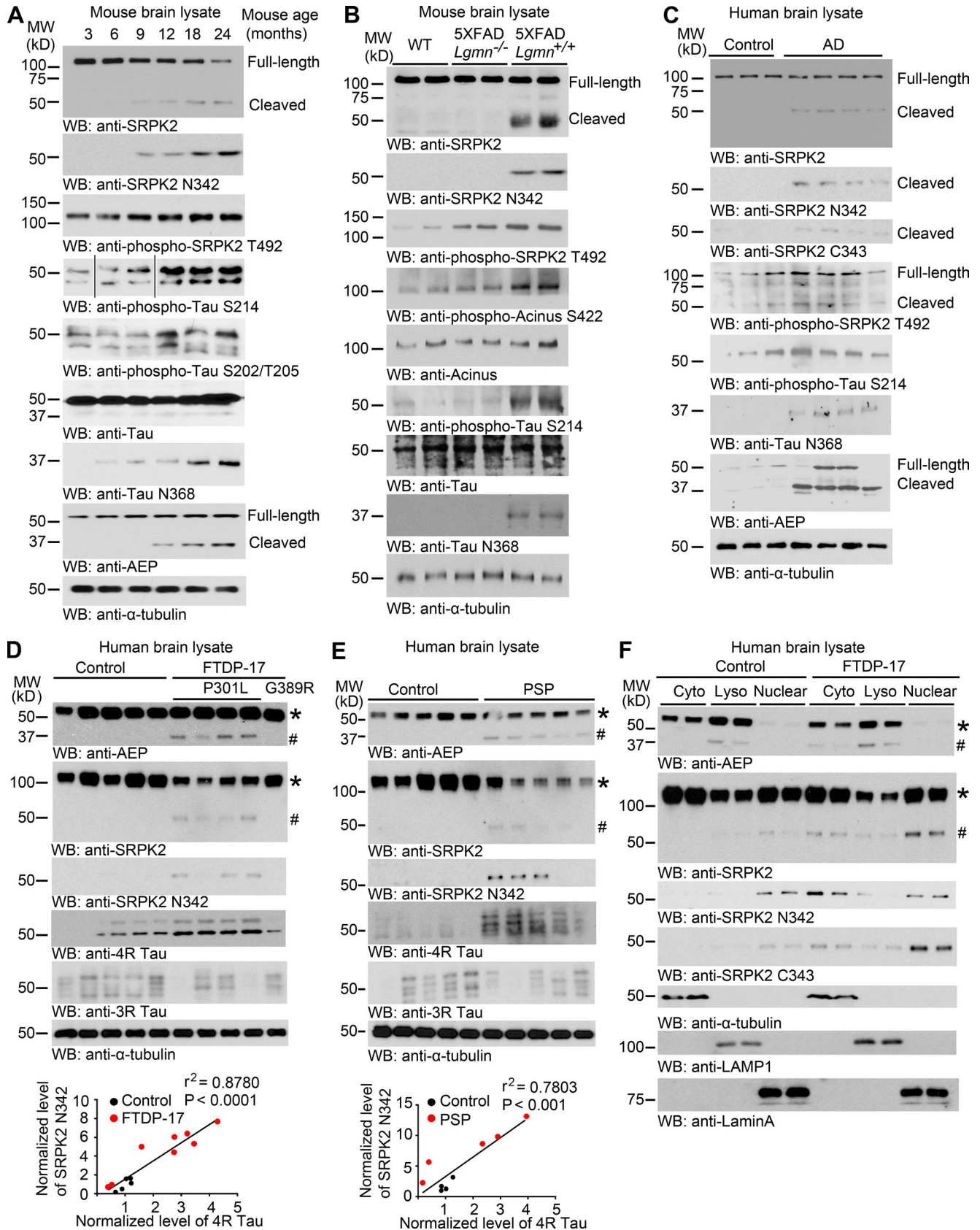


Figure 2. **AEP cleaves SRPK2 during aging and in tauopathies. (A)** Western blot analysis of SRPK2 and AEP in mouse brain during the aging process. SRPK2 activation (p-T492) and its cleavage (SRPK2 N342 and Tau N368) by active AEP were escalated as the age escalation and so were SRPK2 kinase activities (p-tau S214). **(B)** Western blot detection of SRPK2 fragments in 15-mo-old WT, 5XFAD/*Lgmn*^{-/-} and 5XFAD/*Lgmn*^{+/+} mouse brain. Knockout of AEP in 5XFAD mice abolished both SRPK2 N342 and tau N368 cleavage by AEP, diminishing SRPK2 kinase activities on phosphorylation of acinus S422 and tau S214. **(C–E)** Western

fractions upon insoluble tau stimulation (Fig. 3 D). Reverse transcription (RT) PCR analysis showed that tau exon 10 inclusion was increased in response to insoluble tau as compared with buffer or soluble tau (Fig. 3, E and F). Remarkably, AEP enzymatic activities in SH-SY5Y cells were enhanced by insoluble tau, consistent with demonstrable SRPK2 N342 fragmentation by AEP (Fig. 3 G).

Truncated SRPK2 promotes and uncleavable mutant reduces tau exon 10 inclusion

To investigate whether SRPK2 regulates tau exon 10 pre-mRNA splicing, we transfected HEK293 cells with tau exon 10 containing mini-gene (pCI-SI9-SI10) in the presence of WT SRPK2 or truncated SRPK2 1-342 or C343-688 or uncleavable N342A mutant. Quantitative inclusion/exclusion of exon 10 revealed SRPK2 WT almost doubled the inclusion compared to control. The N-terminal SRPK2 1-342 fragment elevated the ratio more than sixfold, and the C-terminal 343-688 truncate augmented approximately two to three times. In contrast, N342A barely increased the inclusion (Fig. 4 A). TaqMan Real-Time PCR Assay for the specific detection and quantification (Connell et al., 2005) of 3R- and 4R-tau confirmed that cleaved SRPK2 regulated tau exon 10 pre-mRNA splicing (Fig. 4 B). As expected, depletion of SRPK2 reduced the inclusion (Fig. 4, C and D). We made the similar observations with endogenous tau in dopaminergic cell line SH-SY5Y and primary neurons (Fig. 4, E-G). In alignment with the splicing results, immunoblotting demonstrated that both 1-342 and 343-688 fragments increased 4R-tau and repressed 3R-tau, fitting with the exon 10 inclusion/exclusion data (Fig. 4 H). As expected, both SC35 and ASF were strongly phosphorylated by the fragmented SRPK2 truncates with N-terminal 1-342 stronger than C-terminal 343-688. It is worth noting that uncleavable N342A mutant decreased splicing factor phosphorylation (Fig. 4 I). To test whether SR-splicing factors SC35 and ASF are accountable for SRPK2's tau exon 10-splicing activity or not, we knocked down SC35 or ASF or their combination with the specific siRNAs in SY5Y cells, respectively, in the presence of SRPK2 FL or AEP-truncated fragments. Quantitative analysis of exon 10 inclusion/exclusion showed that depletion of SC35 or ASF reduced the ratios, and the maximal effect occurred when both factors were depleted. These effects were most prominent in the presence of 1-342 fragment, followed by 343-688, and WT SRPK2 exhibited the modest effect (Fig. 5, A-C). Immunoblotting analysis with the cell lysates revealed the similar results. N-terminal 1-342 strongly increased 4R-tau, which was decreased when either SC35 or ASF was depleted, and the weakest 4R-tau was detected when both factors were knocked down. The similar pattern applied to C-terminal 343-688 fragment and SRPK2 WT. Conversely, 3R-tau was the minimum in the presence of 1-342, in agreement with its strongest activity in promoting exon

10 inclusion. As the splicing factor was knocked down, 3R-tau were elevated and climaxed when both were depleted. The same effect occurred to SRPK2 C-terminal 343-688 fragment as well (Fig. 5 D). Thus, these observations are consistent with the previous report that active SRPK2 translocates into the nucleus, phosphorylating SR-splicing factors including SC35 and ASF (Jang et al., 2009). Together, these data strongly suggest that AEP-cleaved SRPK2 escalates tau exon 10 inclusion via phosphorylating SC35 and ASF pre-mRNA-splicing factors.

AEP-cleaved SRPK2 increases 4R-tau and decreases cognitive functions in htau mice

MAPT (WT htau) transgenic mice lack endogenous mouse tau and express mostly 3R-human tau (Andorfer et al., 2003). The htau mice develop tau pathology in a time course and distribution that is comparable to that occurring in the early stages of human AD. Hyperphosphorylated, conformational altered tau accumulates in the cell bodies and dendrites of neurons in htau mice as they age (Andorfer et al., 2003). To explore whether up-regulating 4R-tau in htau mice via increasing exon 10 inclusion would affect tau pathology and cognitive behaviors or not, we injected lentivirus (LV)-expressing GFP-tagged SRPK2 FL, N-terminal 1-342, or C-terminal 343-688 into the hippocampus of 2-mo-old htau mice, respectively. In 3 mo, we conducted immunoblotting to examine 3R- and 4R-tau expression in the hippocampus. Consequently, SRPK2 FL stimulated 4R-tau expression as compared with GFP control. As expected, the kinase fragments greatly elevated 4R-tau with N-terminal 1-342 stronger than C-terminal 343-688 domain. Inversely, 3R-tau was reduced when the truncated kinase domains were expressed with N-terminal 1-342 more robust than C-terminal 343-688 (Fig. 6 A, first through fifth panels from the top). To test whether different tau isoforms could aggregate into insoluble inclusion, we conducted protein fractionation with Sarkosyl detergent buffer. Notably, 4R-tau was highly distributed in the soluble fraction from truncated kinase domain-injected samples with 343-688 stronger than 1-342. However, 1-342-induced 4R-tau was more prominent in Sarkosyl-insoluble fraction compared with 343-688 (Fig. 6 A, sixth through eleventh panels from the top). RT-PCR analysis of exon 10 inclusion/exclusion ratios showed that 1-342 fragment largely increased the inclusion and decreased exclusion, followed by 343-688 truncation, in alignment with 4R-tau protein level augmentation by these two truncated kinase domains (Fig. 6, B and C). Immunohistochemistry (IHC) staining with AT8 and AT100 indicated that tau was highly phosphorylated in 1-342-injected hippocampus, followed by 343-688, whereas AT8 and AT100 signals were modest in GFP control or WT-injected brains. This was validated with silver staining as well (Fig. 6 D and Fig. S5, A and B). Golgi staining revealed that the dendritic spines in the hippocam-

blot detection of proteolytic truncated SRPK2 fragments and active AEP in human brain samples from subjects with tauopathies including AD (C), FTDP-17 (D), PSP (E), and age-matched controls. The abundance of 3R- and 4R-tau in FTDP-17 and PSP appeared inversely correlated. Bottom in D and E, cleavage of SRPK2 directly correlates with the 4R-tau level in human brain. The Spearman correlation coefficient r^2 and P value are shown. (F) Distribution of SRPK2 fragments in cytosolic, lysosomal, and nuclear fractionations of FTDP-17 human brain samples. The truncated SRPK2 C-terminal fragment C343 appeared highly enriched in the nuclear fraction. Western blot data in A-F are representative of three independent experiments. Three more cases of FTDP-17 are not shown. WB, Western blot; *, FL; #, cleaved SRPK2.

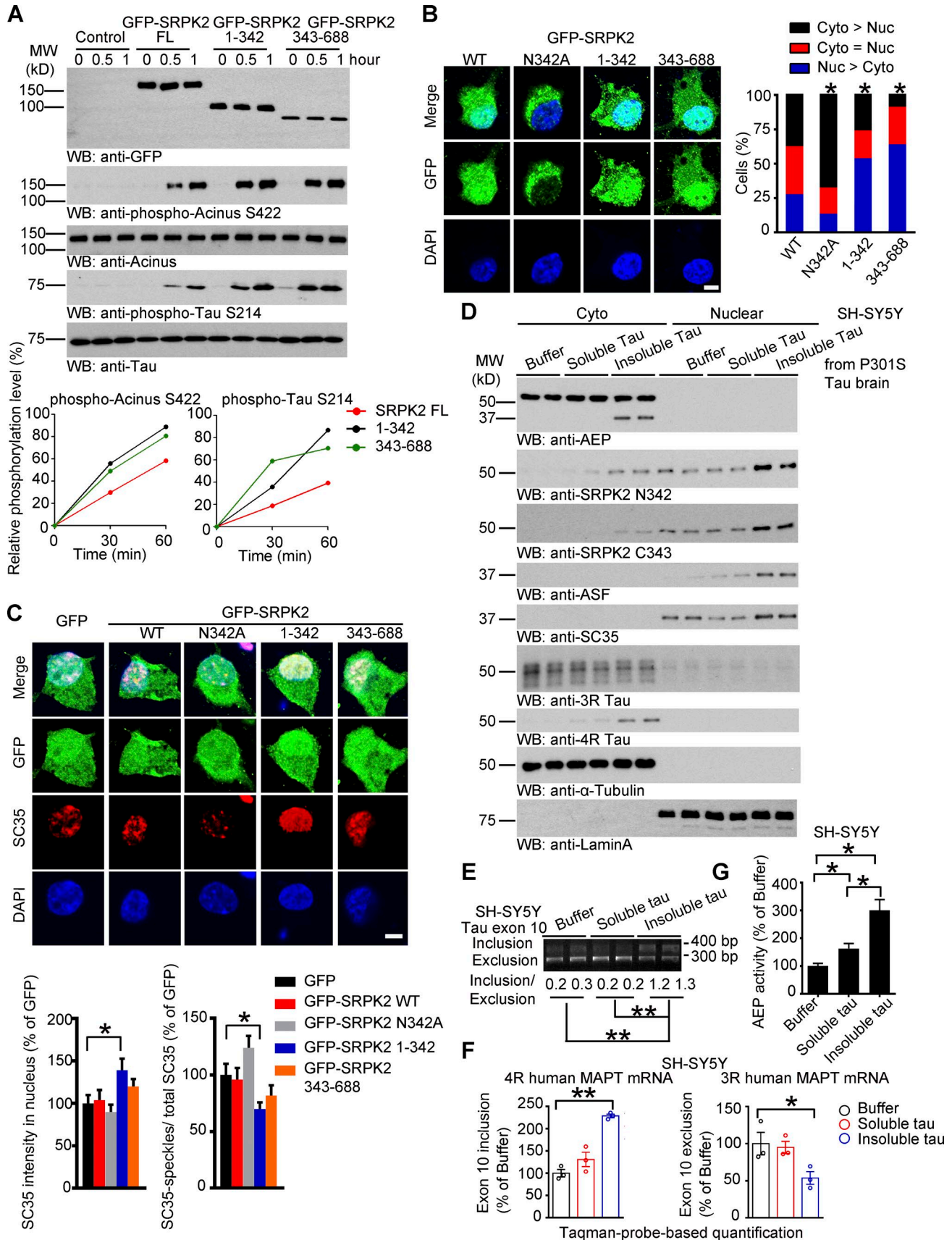


Figure 3. **Cleavage of SRPK2 by AEP promotes its kinase activity and nuclear localization.** (A) Analysis of SRPK2 kinase activity. SRPK2 activity was shown by Western blot after purified GFP-SRPK2 FL, 1-342, or 343-688 was incubated with purified acinus or tau at different time points. Both N-terminal and C-terminal kinase domains from truncated SRPK2 revealed higher kinase activities than FL counterpart. (B) SRPK2 truncation mediates its subcellular residency.

pus were significantly diminished upon 1–342 infection as compared with GFP control (Fig. 6 E). Electronic microscopy (EM) analysis showed that the synapses were substantially reduced in both 1–342 and 343–688 fragment-infected brains compared with control or SRPK2 FL (Fig. S5 C).

LTP is a cellular electrophysiological model for learning and memory. The LTP of field excitatory postsynaptic potentials (fEPSPs) in the hippocampal CA1 region was decreased in N-terminal 1–342-expressed brain compared with control or SRPK2 WT-infected samples (Fig. 6 F). In addition, we examined the synaptic properties in virus-injected htau mice by testing the paired-pulse ratio (PPR), which is a form of short-term plasticity usually used as a measure of the probability of transmitter release. PPR was not greatly affected by SRPK2 WT expression. However, electrophysiological impairment was worsened by 1–342 as PPR was significantly reduced as compared with GFP control. To examine the spatial learning and memory, we conducted the Morris Water Maze (MWM) behavioral test. During the cued platform version of MWM, the mice learned to find the visible platform with the latency reduction. Notably, 1–342-infected mice displayed the slowest learning ability among the four groups (Fig. 6 G, left). A probe trial with hidden platform found that 1–342-overexpressed mice exhibited the poorest memory, illustrated by the fewest time in the platform quadrant (Fig. 6 G, right). The swimming speeds during the hidden platform test in MWM were similar among the groups, indicating that no motor defects occurred in any of the tested mice (Fig. S5 D). Cued fear condition behavioral test showed that the mice infected with SRPK2 1–342 fragment also exhibited the poorest memory among the four groups (Fig. S5 E). Nesting activity is impaired in htau mice with 3R-tau to 4R-tau splicing (Schoch et al., 2016). In alignment with this finding, we showed that the weight of untorn nestlet was the highest in 1–342-infected mice among the groups, indicating the most defective nesting ability (Fig. 6 H). Hence, our data support that AEP-truncated SRPK2 1–342 fragment strongly promotes tau exon 10 inclusion and increases 4R-tau protein levels, resulting in synaptic dysfunctions and impaired cognitive functions and nest building ability.

Uncleavable SRPK2 mutant increases 3R-tau and improves cognitive behaviors in FTDP-17 mutant transgenic mice

A mouse model of FTDP-17 harboring a tau intron 10 +16C→T mutation (609 line) increases tau exon 10 splicing (Hutton et al., 1998) and induces imbalance of 3R- and 4R-tau, triggering the onset of tauopathies (Umeda et al., 2013). This mutation has been

shown to cause an accumulation of 4R-tau in insoluble fractions in patient brains (Goedert et al., 1999; Pickering-Brown et al., 2002). To further explore the pathological role of SRPK2 in tau exon 10 pre-mRNA splicing, we injected LV expressing AEP-uncleavable SRPK2 (N342A) or SRPK2 1–342 into the hippocampus of 609 mouse line and compared tau alternative splicing with control GFP or SRPK2 WT. Remarkably, N342A mutant strongly elevated 3R-tau and decreased 4R-tau; accordingly, 4R-tau was evidently reduced in both Sarkosyl soluble and insoluble fractions as compared with GFP or SRPK2 WT (Fig. 7 A). RT-PCR analysis of the hippocampal mRNA also demonstrated the exclusion augmentation by uncleavable SRPK2 N342A mutant (Fig. 7 B). Thus, the blockade of SRPK2 cleavage by AEP increases tau exon 10 exclusion, up-regulating 3R-tau expression. Consequently, IHC staining with AT8 and AT100 revealed that tau pathological phosphorylation was significantly alleviated in N342A-expressing brains compared to in GFP or SRPK2 WT-infected brains (Fig. 7 C). In contrast, lentiviral expression of SRPK2 N1–342 promoted 4R expression and tau pathological phosphorylation in 609 mice (Fig. 7, A–D). Golgi staining supported that the dendritic spines were more prominently escalated in SRPK2 N342A-infected brains than GFP or SRPK2 WT-expressing samples (Fig. 7 E). EM analysis indicated that SRPK2 N342A notably increased the synapses in the hippocampus comparing with GFP or SRPK2 WT (Fig. S5 F). As a result, electrophysiology assay demonstrated that overexpression of uncleavable SRPK2 N342A significantly augmented the LTP compared to mice expressing GFP or SRPK2 WT (Fig. 7 F). Accordingly, MWM cognitive behavioral test revealed that SRPK2 N342A more substantially improved the cognitive functions in 609 mice than those expressing GFP or SRPK2 WT (Fig. 7 G), though the swim speed rates were comparable among the groups, suggesting that the motor functions were not altered by these proteins overexpressed in the hippocampus (Fig. S5 G). In alignment with the improved learning and memory performances by N342A group in water maze test, contextual fear-conditioning assay showed the similar findings (Fig. S5 H), though there was no discernable difference in the nest-building capability among these groups (Fig. 7 H). Conversely, lentiviral expression of SRPK2 N1–342 exacerbated cognitive impairment in 609 mice (Fig. 7 G). Together, our data support that AEP-uncleavable SRPK2 N342A represses tau exon 10 inclusion splicing and elevates 3R-tau expression, resulting in tau NFT pathology alleviation and cognitive functions improvement in tau intronic 10 +16C→T mutation FTDP-17 mice.

Nuclear/cytosolic localization of FL or truncated GFP-tagged SRPK2. Rat primary neurons were infected with various LV expressing GFP-SRPK2 fusion proteins. Left, localization of SRPK2 was visualized by GFP under fluorescent microscopy. Bars, 5 μ m. Right, percentage of cells exhibiting predominantly nuclear (Nuc > Cyto), predominantly cytoplasmic (Cyto > Nuc), or equivalent nuclear and cytoplasmic (Cyto = Nuc) GFP signal. Three individual experiments were performed, and at least 100 total cells were counted for each condition. Pairwise comparisons between WT protein and each mutant were performed using the χ^2 test (*, $P < 0.001$). (C) Immunofluorescent analysis of SC35 distribution in rat primary neurons infected with various LV expressing GFP-SRPK2 fusion protein. Bar, 5 μ m. Bar graph shows data as mean \pm SEM; $n = 15$ –18 neurons; *, $P < 0.05$; one-way ANOVA. (D) Western blot showing Sarkosyl-insoluble tau induced AEP activation, accompanied with increased SRPK2 truncation, and expression of 4R-tau in SH-SY5Y cells. (E) RT-PCR analysis of human *MAPT* mRNA in 4R to 3R *MAPT* splicing in SH-SY5Y cells upon soluble and insoluble tau treatment. **, $P < 0.01$; one-way ANOVA. (F) TaqMan probe-based quantification of 4R and 3R human *MAPT* mRNA in SH-SY5Y cells upon soluble and insoluble tau treatment. Data represent mean \pm SEM of three independent experiments; *, $P < 0.05$, **, $P < 0.01$; one-way ANOVA. (G) AEP activity assay. The enzymatic activities of AEP in SH-SY5Y cells treated with the indicated conditions were analyzed. Data represent mean \pm SEM of three independent experiments; *, $P < 0.05$; one-way ANOVA. Western blot data in A and D are representative of three independent experiments. MW, molecular weight; WB, Western blot.

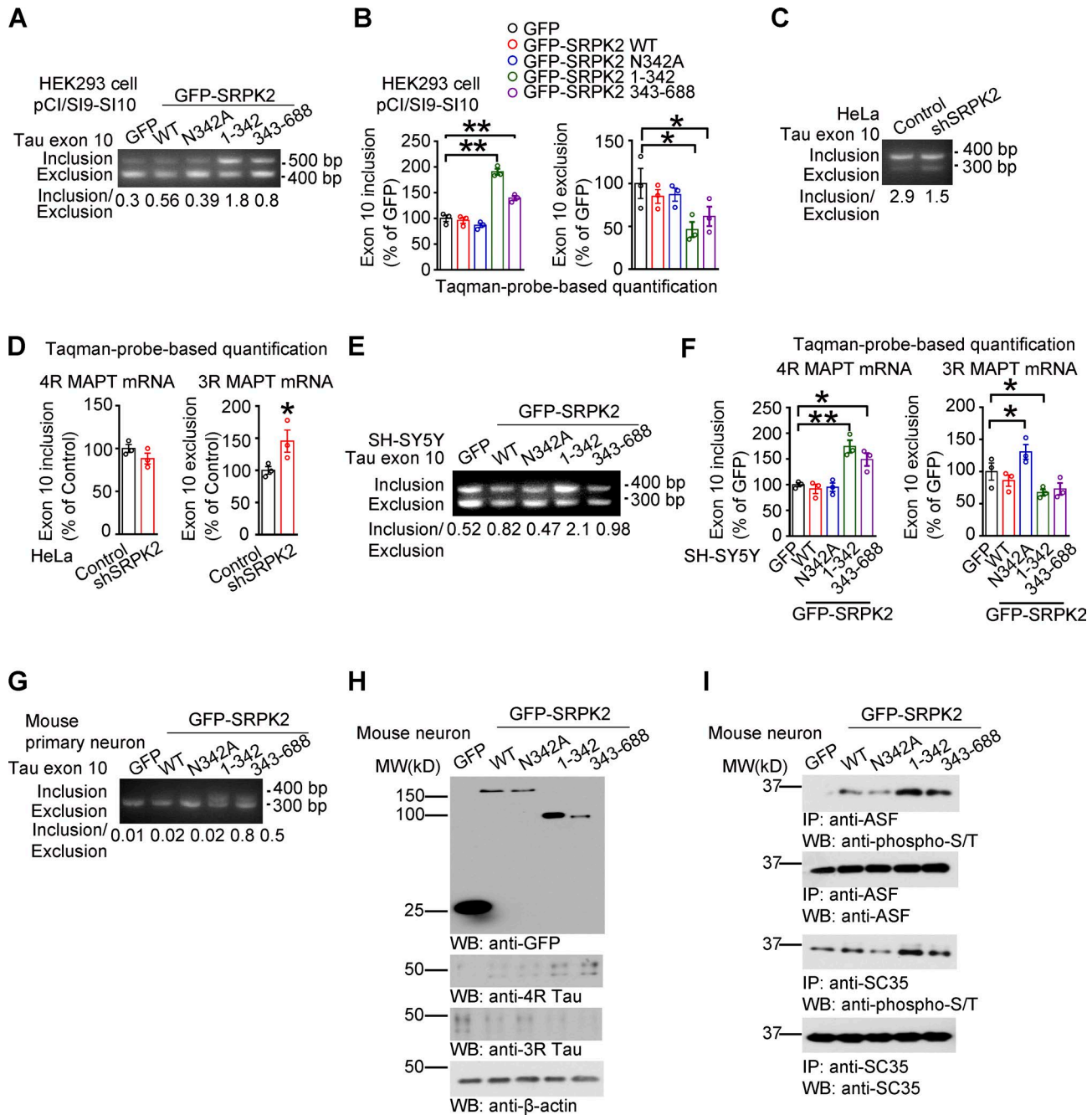


Figure 4. **SRPK2 cleavage by AEP promotes tau exon 10 inclusion.** (A) AEP-truncated SRPK2 promoted tau exon 10 inclusion. The pCI/SI9-SI10 mini-gene of *MAPT* was transfected with into HEK293 cells infected with virus expressing various indicated SRPK2 constructs. Total RNA was subjected to RT-PCR for measurement of tau exon 10 splicing 36 h after transfection. Both N-terminal and C-terminal kinase domains of SRPK2 displayed elevated effect in augmenting exon 10 inclusion compared with SRPK2 FL counterpart. (B) TaqMan probe-based quantification of tau exon 10 inclusion and exclusion in HEK293 cells co-expressing pCI/SI9-SI10 mini-gene and SRPK2. Data represent mean ± SEM of three independent experiments; *, P < 0.05; **, P < 0.01; one-way ANOVA. (C and D) Knockdown of SRPK2 by its shRNA-suppressed tau exon 10 inclusion in HeLa cells. Data in D represent mean ± SEM of three independent experiments; *, P < 0.05; two-tailed Student's *t* test. (E-G) RT-PCR analysis of 4R to 3R *MAPT* splicing in SH-SY5Y cells (E and F) and neurons (G) infected with LV expressing WT, uncleavable (N342A), or cleaved SRPK2 fragments (1-342 and 343-688). Data in F represent mean ± SEM of three independent experiments; *, P < 0.05, **, P < 0.01; one-way ANOVA. (H and I) Western blot showing SRPK2 cleavage increased ratio of 4R-/3R-tau protein expression levels (H) and phosphorylation of splicing factors ASF and SC35 (I) in neurons. Data in A, C, E, G, and H are representative of three independent experiments. IP, immunoprecipitation; WB, Western blot.

Discussion

In the current study, we show that AEP cleaves SRPK2 at multiple locations with N342 residue the major site. The bipartite kinase catalytic core in SRPK2 is separated by a unique spacer sequence

(Ding et al., 2006). Cleavage of SRPK2 by AEP separates its two kinase domains and escalates the kinase activities in tauopathy brains. Notably, N-terminal SRPK2 1-342 elevates tau exon 10 inclusion and up-regulates 4R-tau expression levels in *MAPT* mice,

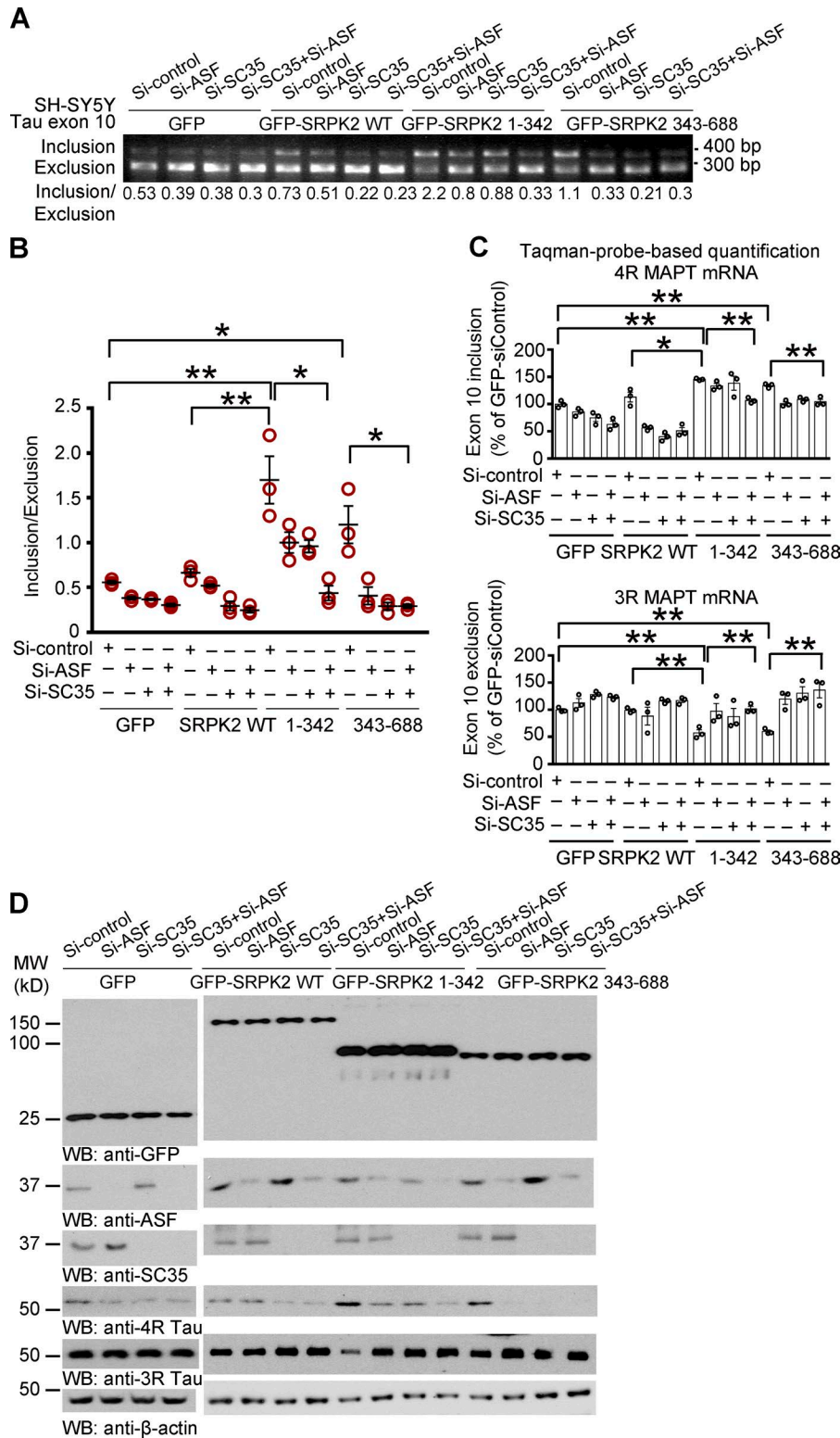
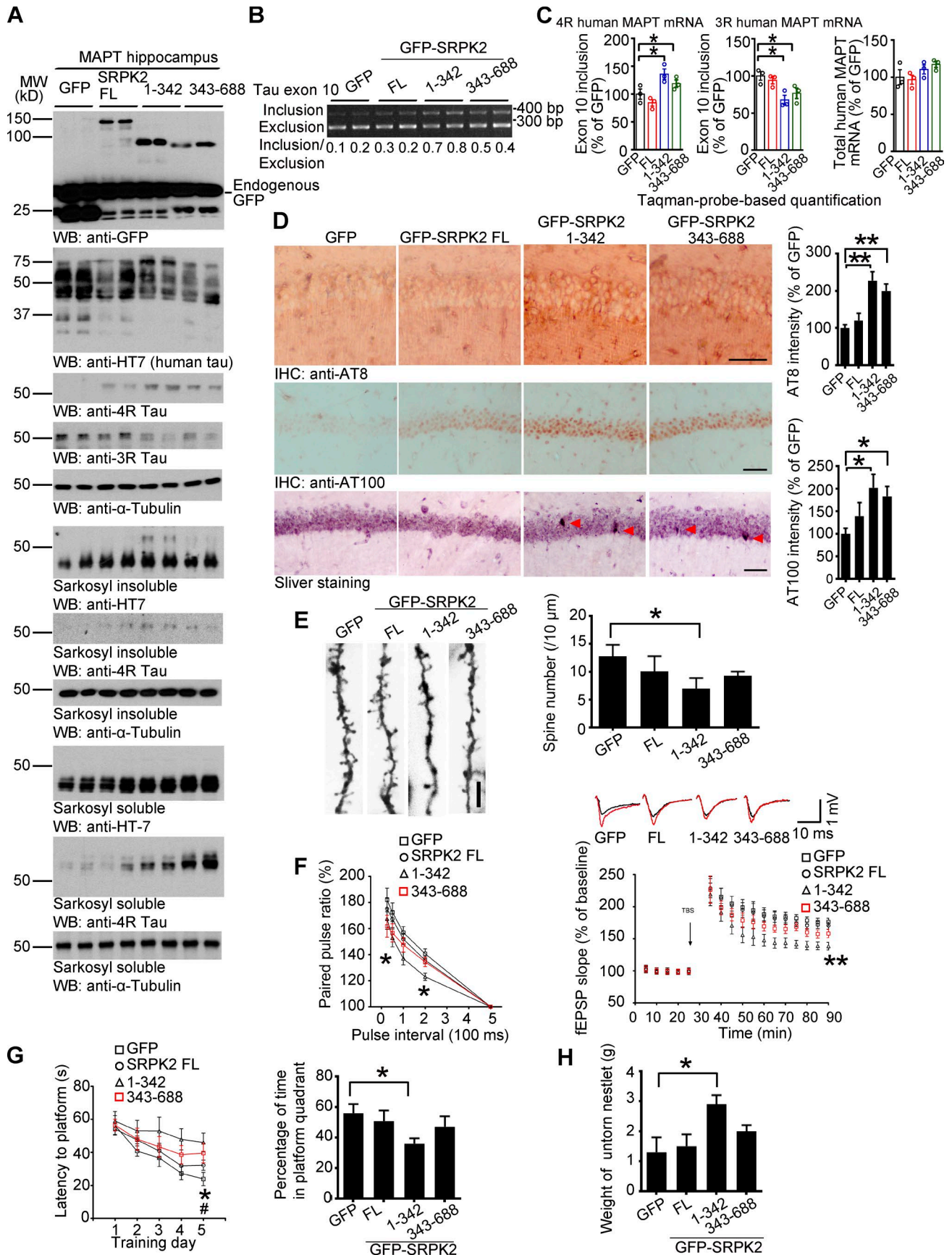


Figure 5. **Knockdown of ASF and SC35 suppressed tau exon 10 inclusion induced by SRPK2 cleavage.** (A and B) RT-PCR analysis showing knockdown of ASF and SC35 suppressed tau exon 10 inclusion induced by AEP-cleaved SRPK2 in SH-SY5Y cells. Data in B represent mean \pm SEM of three independent experiments; *, $P < 0.05$; **, $P < 0.01$; one-way ANOVA. (C) TaqMan probe-based quantification of tau exon 10 splicing. Data represent mean \pm SEM of three independent experiments; *, $P < 0.05$; **, $P < 0.01$; one-way ANOVA. (D) Western blot showing knockdown of ASF and SC35 suppressed the increase in 4R/3R ratio in SH-SY5Y cells transfected with cleaved SRPK2. Data in A and D are representative of three independent experiments. MW, molecular weight; WB, Western blot.

accelerating tau pathologies and cognitive impairments in young htau mice. On the other hand, uncleavable SRPK2 N342A mutant facilitates tau exon 10 exclusion and augments 3R-tau expression levels in FTDP-17 mice, reversing tau pathologies and ameliorating cognitive dysfunctions. In addition to the major function as an SR protein kinase, SRPK2 is involved in the cell cycle regulation, cell proliferation, and neuronal apoptosis (Jang et al., 2009;

Giannakouros et al., 2011). Our previous study demonstrates that SRPK2 directly phosphorylates tau on S214 residue and suppresses its MT-binding affinity in AD brains (Hong et al., 2012). Here, we provide extensive evidence supporting that SRPK2 also regulates tau exon 10 alternative splicing in tauopathies via phosphorylating SR-splicing factors including SC35 and ASF/SF2 proteins. Clearly, AEP-cleaved SRPK2 fragments translocate into the nucleus, and



we found that the nuclear translocation of both fragments is comparable as shown by subcellular fractionation in Fig. 3 D, though SRPK2 C343–688 appears a little bit more than SRPK2 N1–342 (Fig. 3 B). However, the nucleus is not the only location where SRPK2 phosphorylates SC35/ASF. In the cytoplasm, phosphorylation of SC35/ASF by active SRPKs leads to nuclear translocation of SC35/ASF, promoting alternative splicing (Liu and Gong, 2008; Zhong et al., 2009). Noticeably, the phosphorylation of SC35 by the cytoplasmic SRPK2 N1–342 elicits much more SC35 to the nucleus (Fig. 3 C), leading to a stronger increase of 4R-tau than SRPK2 C343–688. Further, as shown in Fig. 3 A, SRPK2 N1–342 fragment exhibits higher kinase activity than SRPK2 C343–688, which may also contribute to a more robust phosphorylation of splicing factors SC35/ASF and more abundant 4R-tau expression (Fig. 4 and Fig. 5). Though both fragments triggered AT-8-positive and NFT pathologies in young htau mice, N-terminal 1–342 mice display significantly worse synaptic plasticity and cognitive dysfunctions as compared with C-terminal SRPK2 343–688 fragment (Fig. 5), consistent with its higher activity in phosphorylating both ASF- and SC35-splicing factors and more abundant 4R-tau.

Dysregulation of tau exon 10 splicing causes neurodegenerative diseases (Yen et al., 1999; Ingram and Spillantini, 2002; Umeda et al., 2013). Tau isoforms are balanced with approximately equal ratio of 3R/4R in normal adult human brain; imbalances in 3R/4R ratio have been tightly associated with the pathogenesis of several neurodegenerative diseases, yet the underlying molecular mechanisms remain elusive (Lacovich et al., 2017). Alternative splicing of tau exon 10 is regulated by splicing factors acting on the cis-elements located mainly on exon 10 and intron 10 (Hartmann et al., 2001; Qian et al., 2011). These splicing factors include serine- and arginine-rich (SR) proteins and heterogeneous nuclear ribonucleoproteins as well as tissue-specific factors (Manley and Krainer, 2010). Numerous SR proteins, including SRp55, 9G8, SC35, and ASF/SF2, mediate the alternative splicing of tau exon 10 (Qian et al., 2011; Shi et al., 2011; Ding et al., 2012; Gu et al., 2012). In this regard, one such SR protein is SC35, which promotes exon 10 inclusion by acting on a SC35-like enhancer at the 5' end of the tau RNA transcript (Qian et al., 2011). Interestingly, phosphorylation of SC35 by protein kinase A enhances inclusion of exon 10, resulting in increased expression

of the 3R-tau isoform (Chen et al., 2014). Inclusion of exon 10 generating 4R-tau isoform can lead to enhanced NFTs and tau aggregation (Goedert et al., 1989). In addition to protein kinase A, dual-specificity tyrosine-phosphorylated and regulated kinase 1A (DYRK1) also mediates tau exon 10 splicing via phosphorylating various SR proteins (Shi et al., 2008; Qian et al., 2011; Ding et al., 2012). Here, we show that AEP-truncated SRPK2 translocates into the nucleus, where it strongly phosphorylates SR-splicing factors (e.g., SC35 and ASF/SF2) and regulates tau exon 10 splicing (Fig. 4). Recently, we reported that SRPK2 phosphorylates tau and suppresses tau-dependent MT polymerization, inhibiting axonal elongation in neurons. Depletion of SRPK2 in dentate gyrus inhibits tau phosphorylation in APP/PS1 mouse and improves the defective LTP, alleviating the impairments in cognition. Moreover, active SRPK2 is increased in APP/PS1 mice and human AD brains (Hong et al., 2012). Plausibly, abnormal activation of SRPK2 may phosphorylate numerous substrates including AEP (Wang et al., 2017), tau (Hong et al., 2012), and SR domain-containing splicing factors including acinus (Jang et al., 2008), coordinating the aberrant AD pathologies.

The RNA splicing is performed by the massive protein complex, the spliceosome, which consists of small nuclear ribonucleoproteins (snRNP) and a range of associated splicing regulatory factors (Kornblihtt et al., 2013). A comprehensive study of the human brain-insoluble proteome in AD by mass spectrometry has recently been reported. Among thousands of proteins identified, 36 proteins accumulate in AD brains, including U1-70K and other U1 snRNP spliceosome components. Similar accumulation in mild cognitive impairment (cases indicates that spliceosome changes occur in early stages of AD). Multiple U1 snRNP subunits including U1-70K and U1A form cytoplasmic tangle-like structures in AD but not in other neurodegenerative disorders (Bai et al., 2013; Hales et al., 2014). Consequently, evidence of widespread alterations in RNA processing in human AD brains has been observed, suggesting that disruption of neuronal RNA processing may play a key role in AD pathogenesis (Bai et al., 2014). Phosphorylation of a SR protein (ASF/SF2) by either SRPK1 or SRPK2 enhances its interaction with U1-70K, and overexpression of either kinase induces specific redistribution of splicing factors in the nucleus. These observations indicate a function of SRPK family of kinases

Figure 6. Expression of AEP-truncated SRPK2 in young MAPT mice hippocampal CA1 accelerates the onset of tau pathogenesis and worsens cognitive dysfunctions. (A) Western blot analysis of ratio of 4R-/3R-tau expression and Sarkosyl-insoluble or soluble tau levels in MAPT (WT htau) mice CA1 infected with LV expressing SRPK2 fragments. AEP-cleaved SRPK2 fragments elevated 4R-tau and repressed 3R-tau expression levels. The increased 4R-tau was mainly distributed in Sarkosyl soluble fraction. Data are representative of three independent experiments. (B) RT-PCR analysis of tau exon 10 splicing in cleaved SRPK2-expressed htau mice CA1. AEP-truncated SRPK2 escalated tau exon 10 inclusion. (C) TaqMan probe-based quantification of tau exon 10 splicing. Data represent mean \pm SEM of three mice in each group (*, $P < 0.05$; one-way ANOVA). (D) Detection of phosphorylated and aggregated tau in cleaved SRPK2-expressed htau mice. Top and middle, IHC staining of tau phosphorylation AT8 and AT100. Bottom, Gallyas silver staining. AEP-truncated SRPK2 increased tau pathological phosphorylation and aggregation compared with SRPK2 FL. Bar, 25 μ m. Data represent mean \pm SEM of 9–12 sections from three mice in each group (*, $P < 0.05$; **, $P < 0.01$; one-way ANOVA). (E) SRPK2 cleavage by AEP decreases the dendritic spine density. Left, Golgi staining was conducted on brain sections from LV-GFP/ SRPK2 WT or truncated SRPK2 treated apical dendritic layer of the CA1 region. Bar, 5 μ m. Right, quantification of spine density represents mean \pm SEM of 9–12 sections from three mice in each group (*, $P < 0.05$; one-way ANOVA). (F) Electrophysiology analysis. Truncated SRPK2 (1–342) expression in CA1 worsened the LTP defects in htau mice. The ratio of paired pulses in different groups (mean \pm SEM; $n = 6$ in each group; *, $P < 0.05$ compared with htau-GFP; one-way ANOVA; left). LTP of fEPSPs (mean \pm SEM; $n = 6$ in each group; *, $P < 0.05$ htau-SRPK2 1–342 vs. htau-GFP; **, $P < 0.01$, htau-SRPK2 1–342 vs. htau-GFP; one-way ANOVA; right). The traces are representative fEPSPs recorded before (black) and 60 min after (red) TBS. (G) MWM analysis of cognitive functions. AEP-cleaved SRPK2 expression in the CA1 exacerbated the learning and memory dysfunctions in htau mice (mean \pm SEM; $n = 8$ –10 mice per group; *, $P < 0.05$; #, $P < 0.05$, htau-SRPK2 343–688 vs. htau-GFP one-way ANOVA). (H) Nesting activity analysis. Cleaved SRPK2-expressed htau mice exhibited significantly greater untorn nestlet weights indicative of poor nesting activity compared with GFP (mean \pm SEM; $n = 8$ –10 mice per group; *, $P < 0.05$; one-way ANOVA). MW, molecular weight; WB, Western blot.

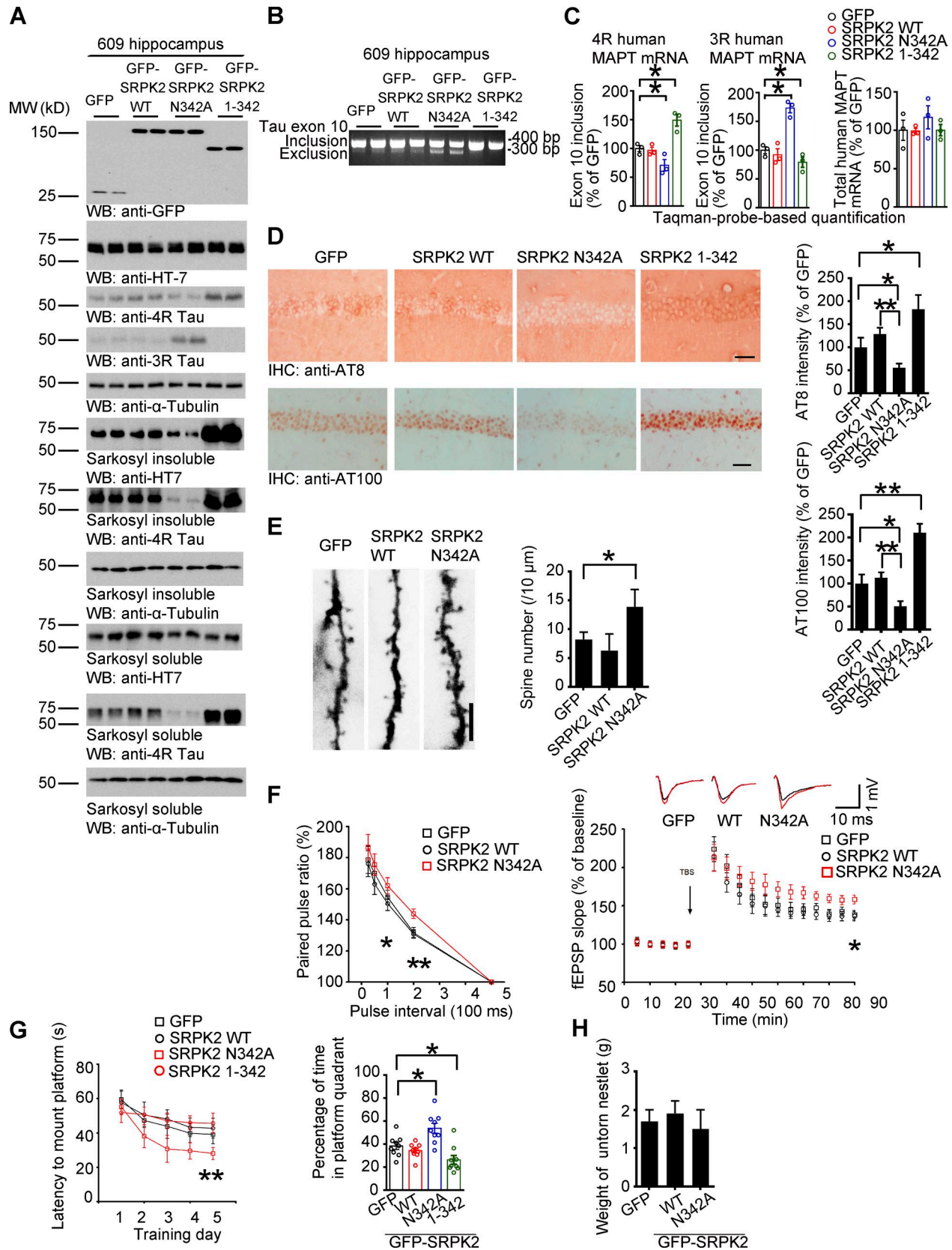


Figure 7. **Blocking of SRPK2 cleavage by AEP prevents 4R-tau-induced synaptic dysfunction and cognitive impairment.** (A) AEP-uncleavable SRPK2 mutant (N342A) represses 4R-tau expression and SRPK2 1-342 promotes 4R-tau in *MAPT* intronic mutated FTDP-17 mouse model. Western blot analysis of ratio of 4R-/3R-tau expression and Sarkosyl-insoluble or soluble tau levels in tau609 mice CA1-infected with LV expressing SRPK2 WT, N342A or 1-342. (B) RT-PCR analysis of tau exon 10 splicing in SRPK2 WT/N342A/1-342-expressed tau609 mice CA1. (C) TaqMan probe-based quantification of tau exon 10 splicing. Data represent mean \pm SEM of three mice in each group. *, $P < 0.05$; one-way ANOVA. (D) IHC staining of phosphorylated tau in tau609 mice CA1 expressing

in spliceosome assembly and in mediating the trafficking of splicing factors in mammalian cells (Wang et al., 1998). Conceivably, A β -activated SRPK2 may phosphorylate SR proteins and elicit their association with U1-70K, leading to the cytoplasmic accumulation in AD brains. The abnormal distribution may trigger global RNA processing defects in AD etiology. Remarkably, U1-70K knockdown or antisense oligonucleotide inhibition of U1 snRNP increases the protein level of APP (Bai et al., 2013). Imaginably, SRPK2 may also influence APP metabolism via mediating U1-70K trafficking (Chan and Ye, 2013), in addition to affecting the enzymatic activity of AEP via phosphorylation (Wang et al., 2017).

Tau intronic mutant mice (609 line) display the pathological abnormalities induced just by changing the 3R-/4R-tau ratio, even in the absence of a missense mutation. Patients with this mutation have been reported to present prominent frontotemporal lobar atrophy with neuronal and glial tau inclusions in the form of NFT and pretangles (Janssen et al., 2002; Lantos et al., 2002; Doran et al., 2007). Using WT htau MAPT and tau intronic 10 +16C→T mutation FTDP-17 (609 line) animal models, we manipulated tau exon 10 alternative splicing by administering AEP-cleaved SRPK2 fragments or uncleavable SRPK2 N342A mutant into the mouse brains, and established that the event of AEP cleavage of SRPK2 plays a critical role in dictating tau exon 10 splicing. Interestingly, AEP-cleaved SRPK2 possesses higher kinase activities and promotes exon 10 inclusion and 4R-tau expression, resulting in neurotoxicity in young MAPT mice. Nonetheless, preventing SRPK2 cleavage by AEP in 609 mice decreases 4R-tau and alleviates tau pathologies, improving the cognitive functions (Fig. 5 and Fig. 6). Conceivably, active AEP in tauopathies may regulate tau splicing via proteolytically truncating SRPK2, which feeds back and phosphorylates AEP on S226, promoting its cytoplasmic translocation from the lysosomes and auto-cleavage and activation (Wang et al., 2017). Presumably, this feed-forward mutual regulation may amplify the detrimental signalings, deteriorating the neurodegenerative pathologies and facilitating the cognitive dysfunctions. Nest building, an important innate behavior of diverse mammalian species, depends on proper functioning of hippocampus and cortex. It has been shown that increased 4R-tau in htau mice elicits abnormal nest building behaviors, showing 4R-tau neurotoxicity (Schoch et al., 2016). Accordingly, augmentation of 4R-tau by overexpressing SRPK2 1–342 sabotaged the nest building ability in htau mice (Fig. 5 G). However, it remains unclear why uncleavable N342A-infected 609 mice that exhibit evidently reduced 4R-tau in Sarkosyl-insoluble fraction do not improve the nesting building capability

(Fig. 7 A, seventh panel from the top), though these mice display significantly alleviated cognitive functions. Probably, the total 4R-tau levels in the hippocampus are not dramatically lowered by N342A mutant as compared with control mice (Fig. 7 A, third panel from the top). However, it is worth noting that 609 mice are not AD mouse models, and it is unwarranted to extrapolate about the role of preventing SRPK2 cleavage by AEP and expression on 4R in the rescue of pathology for tauopathies in general.

It is known that tau exon 10 splicing is developmentally regulated; in fetal brains, 3R-tau is exclusively expressed in rodents and humans; however, in adult brains, 4R-tau expression becomes exclusive in rodents, whereas 3R- and 4R-tau are comparably expressed at a ratio of almost 1:1 in humans (Goedert et al., 1989; Kosik et al., 1989). Thus, mutation-induced alteration of tau exon 10 splicing presumably causes pathological imbalances in 3R- and 4R-tau, potentially leading to neurodegeneration. Although there is no consensus in the field about the imbalance ratio of 3R/4R in AD (Murray et al., 2014), it is clear that unbalanced ratios of 3R/4R occur in diseases such as PSP and corticobasal degeneration. It remains unclear of how imbalance of tau isoforms causes neurodegenerative diseases. The neurodegeneration occurs regardless of which way of the exon 10 tilts. Hence, the balance between 3R and 4R isoforms must remain within a narrow window to ensure normal neuronal functions. Perhaps the 1:1 3R/4R ratio is critical for MT dynamics in specific contexts within various cell types of the human brain, a balancing act between fluidity and stability (Andreadis, 2012). Collectively, our current finding provides innovative insight into the molecular mechanism of how AEP and SRPK2 crosstalk may provoke tau isoform imbalance in various tauopathies.

Materials and methods

Mice, primary cultured neurons, cell lines, and human tissue samples

5XFAD mice, WT C57BL/6J mice, and MAPT mice were ordered from the Jackson Laboratory (stock nos. 006554, 000664, and 005491, respectively). Tau intronic 10 +16C→T mutation FTDP-17 mice (609 line) were a gift from H. Mori (Osaka City University, Osaka, Japan). The *Lgmn*^{-/-} mice on a mixed 129/Ola and C57BL/6 background were generated as previously reported (Shirahama-Noda et al., 2003). *Lgmn*^{-/-} mice were crossed with 5XFAD mice to generate 5XFAD/*Lgmn*^{-/-} mice. In animal experiments related to Fig. 1 (A and D), Fig. 2 B, Fig. 6, Fig. 7, Fig. S2, and Fig. S5, WT

SRPK2 WT, N342A or 1–342. AT8 and AT100 signals were reduced in uncleavable SRPK2 mutant-infected hippocampus and increased in 1–342 group. Bars, 50 μ m. Data represent mean \pm SEM of 9–12 sections from three mice in each group (*, $P < 0.05$; **, $P < 0.01$; one-way ANOVA). (E) Blocking of SRPK2 cleavage by AEP increases the dendritic spine density. Left, Golgi staining was conducted on brain sections from LV-GFP/SRPK2 SRPK2 WT, N342A or 1–342. Treated apical dendritic layer of the CA1 region. Bar, 5 μ m. Right, quantification of spine density represents mean \pm SEM of 9–12 sections from three mice in each group (*, $P < 0.05$; one-way ANOVA). (F) Electrophysiology analysis. Uncleavable SRPK2 (N342A) mutant expression in CA1 rescued the LTP defects in tau609 mice. The ratio of paired pulses in different groups (mean \pm SEM; $n = 6$ in each group; *, $P < 0.05$ tau609-SRPK2 N342A compared with tau609-GFP; **, $P < 0.01$ tau609-SRPK2 N342A compared with tau609-GFP; one-way ANOVA; left). LTP of fEPSPs (mean \pm SEM; $n = 6$ in each group; *, $P < 0.05$ tau609-SRPK2 N342A compared with tau609-GFP; one-way ANOVA; right). The traces are representative fEPSPs recorded before (black) and 60 min after (red) TBS. (G) MWM analysis of cognitive functions. Uncleavable SRPK2 (N342A) mutant expression in the CA1 reversed the learning dysfunctions in tau 609 mice (mean \pm SEM; $n = 8–9$ mice per group; **, $P < 0.01$ tau609-SRPK2 N342A compared with tau609-GFP; one-way ANOVA; left). SRPK2 N342A rescued the impaired memory, while SRPK2 1–342 exacerbated memory impairment in 609 mice (right). Data represent mean \pm SEM of eight to nine mice in each group (*, $P < 0.05$; one-way ANOVA). (H) Nesting activity analysis. There is no significant difference in the three groups. MW, molecular weight; WB, Western blot.

littermate mice were used as controls. Animal care and handling was performed according to National Institutes of Health (NIH) animal care guidelines and Emory Medical School guidelines. The protocol was reviewed and approved by the Emory Institutional Animal Care and Use Committee. Primary cortical neurons were cultured as previously described (Zhang et al., 2014). All rats were purchased from the Jackson Laboratory. The protocol was reviewed and approved by the Emory Institutional Animal Care and Use Committee. HEK293 and HeLa cells were cultured in high-glucose DMEM added with 10% FBS and penicillin (100 U/ml)–streptomycin (100 µg/ml; all from Hyclone). SH-SY5Y cells were cultured in DMEM/F12 added with 10% FBS and penicillin (100 U/ml)–streptomycin (100 U/ml; all from Hyclone). Cells were incubated at 37°C in a humidified atmosphere of 5% CO₂. Postmortem brain samples were dissected from frozen brains of AD, FTDP-17, PSP, and aged-match nondemented controls from the Emory AD Research Center. The study was approved by the Biospecimen Committee. AD was diagnosed according to the criteria of the Consortium to Establish a Registry for AD and the National Institute on Aging. Diagnoses were confirmed by the presence of amyloid plaques and neurofibrillary tangles in formalin-fixed tissue. Informed consent was obtained from the subjects. Diagnosis criteria used for FTDP-17 and PSP brains were assigned using current criteria (Hauw et al., 1994; Foster et al., 1997). Evidence for the presence or absence of silver-positive neuronal tau inclusions are shown in Fig. S3 A. Detailed reagents and resources are provided in Table S1.

Plasmids

FL, truncated, and site-mutated SRPK2 were inserted into pEGFP-C2 between BglII and SalI cutting sites, or into pFCGW-N1 between BamHI and EcoRI cutting sites for LV package. The shRNA sequences targeting SRPK2 were fused into the lentiviral vector pFH1UGW. The sites indicated for tau protein represent the amino acids in the longest form of human tau protein (Tau441). The target sequences recognized by shSRPK2 (5'-GCA GAGAGTGATTACACGTAT-3') were acquired from Sigma-Aldrich MISSION shRNA library. pCI/SI9-SI1 was a gift from F. Liu (New York State Institute for Basic Research in Developmental Disabilities, New York, NY).

LV packaging

LV packaging system (pFCGW-N1) was acquired from the Viral Core Facility of Emory University. Transfection of the lentiviral vectors were performed in HEK293FT cells (50–60% confluent) with calcium phosphate reagents. After 16 h, the transfection media were discarded, and the cells were washed with sterile PBS and incubated with prewarmed fresh culture media. After 48 h incubation, the cell culture media were collected, and the lentiviral particles were concentrated by ultracentrifugation at 22,000 RPM (SW28) for 2 h at 4°C. All the LV-containing materials were handled according to the Biosafety Regulation of Emory University. Viral titer was ~1–5 × 10⁹ IU/ml.

Transfection and infection of the cells

HEK293 transfection was performed using Lipofectamine 2000 (Invitrogen). SH-SY5Y transfection was performed using Lipo-

fectamine 3000 (Invitrogen). The LVs used in neuronal infection were packaged in Viral Vector Core of Emory University.

Quantitation of tau exon 10 splicing by RT-PCR

For cell experiment, total cellular RNA was isolated from cultured cells by using an RNeasy mini kit (Qiagen GmbH). 600 ng of total RNA was used for first-strand CdnA synthesis with oligo (dT)18 by using an Omniscript reverse transcription kit (Qiagen GmbH). PCR was performed by using Prime-STARTTM HS DNA Polymerase (Takara Bio Inc.) with primers (forward, 5'-GGTGTC CACTCCCAGTTCAA-3'; and reverse, 5'-CCCTGGTTTATGATGGAT GTTGCTTAATGAG-3') for human tau in HEK293 cells transfected with pCI/SI9-SI10, and with primers (forward, 5'-CACCAAAAT CCGGAGAACGA-3'; and reverse, 5'-CTTTGCTCAGGTCCACCGGC-3') for mouse tau to measure alternative splicing of tau exon 10 under the following conditions: denaturation for 5 min at 98°C was followed by 30 cycles with denaturation for 10 s at 98°C, annealing for 15 s at 55°C, polymerization for 30 s at 72°C, and a final extension for 10 min at 72°C. The PCR products were resolved on 1.5% agarose gels and quantitated using the Molecular Imager system (Bio-Rad).

For SH-SY5Y cells and MAPT mice mRNA, the sequences of the primers were as follows: forward, 5'-CTCCAAAATCAGGGG ATCGC-3'; and reverse, 5'-CCTTGCTCAGGTCAACTGGT-3'. RT was omitted in control reactions. RT-PCR products were separated in 2% (wt/vol) agarose gels and stained with ethidium bromide. Isoforms were identified based on their expected sizes. Products containing exon 10 (4R) were 390 bp, while those without exon 10 (3R) were 253 bp.

For tau 609 mice, primer sequences used were as follows: human exon 9F, 5'-CTCCAAAATCAGGGGATCGC-3'; and human exon 11R, 5'-CCTTGCTCAGGTCAACTGGT-3'. PCR was performed as 30 cycles at 94°C for 30 s, at 62°C for 30 s, and at 72°C for 45 s, with a final 72°C extension for 10 min. The expected sizes of PCR products were 390 bp for exon 10⁺ mRNA and 297 bp for exon 10⁻ mRNA. Relative amounts of 4R- and 3R-tau RNA were estimated by densitometric analysis of the gels using the ImageJ software (NIH).

TaqMan probe-based quantification

The levels of mRNA were analyzed by real-time, quantitative PCR. RNA was isolated by Trizol (Life Technologies). RT was performed with SuperScriptIII reverse transcription (Life Technologies). Gene-specific primers and probes were designed and bought from TaqMan (Life Technologies).

Changes in MAPT expression were detected quantitative real-time PCR was performed using a ABI 7500-Fast Real-Time PCR System with TaqMan Fast Universal PCR Master Mix and Applied Biosystems TaqMan Gene Expression Assay Mix, ID no. Hs00902194_m1. This probe binds the junction of MAPT exons 12–13; constitutive exons present in all isoforms and therefore this assay helps determine total levels of all MAPT transcripts.

Primers and probes for 3R and 4R human MAPT mRNA were designed as reported (Connell et al., 2005). For 3R isoform detection, the sequences used were as follows: forward, 5'-GAGGCGGAAGGTGCAAAT-3', and reverse, 5'-GGATGTTGC CTAATGAGCCAC-3'; probe, 5'-ACAAACCAGTTGACCTGAGCA AGGTGACCTCC-3'.

For 4R isoform detection, the sequences used were as follows: forward, 5'-GAGGCGGGAAGGTGCAGATAA-3'; and reverse, 5'-GGATGTTGCTAATGAGCCAC-3'; probe, 5'-ACAAACCAGTTGACC TGAGCAAGGTGACCTCC-3'.

The relative quantification of gene expression was calculated as 2-ddCt method. For each data point, at least two duplicated wells were used, and each experiment was repeated at least three times.

Generation of antibodies that specifically recognize the AEP-generated SRPK2 fragment (anti-SRPK2 N342 and anti-SRPK2 C343)

The anti-SRPK2 N342 and anti-SRPK2 C343 antibodies were generated by immunizing rabbits with the following peptides: Ac-CAEAETAKDN-OH (anti-SRPK2 N342) and H2N-GEAEDQ EEKC-amide (anti-SRPK2 C343), respectively. The antiserum was pooled, and the titers against the immunizing peptide were determined by ELISA. The maximal dilution giving a positive response using chromogenic substrate for HRP was >1:30,000. The immunoreactivity of the antiserum was further confirmed by Western blot and IHC.

Subcellular fractionation

The protocol was as previously described (Basurto-Islas et al., 2013). Brain tissue and SH-SY5Y cell lysates were prepared in three volumes of cold homogenizing buffer (0.32 M sucrose, 1 mM EDTA disodium, and 10 mM Hepes, pH 7.4). Lysates were centrifuged at 750 g for 10 min. The supernatant was kept, and the pellet was resuspended and centrifuged. The second supernatant was combined with the previous one, and the pellet was saved as the nuclear fraction. The pooled supernatant was centrifuged at 20,000 g for 10 min. The pellet was saved, the supernatant was centrifuged at 105,000 g for 1 h, and the resulting supernatant was saved as the cytosolic fraction. The 20,000-g pellet from above was resuspended in homogenizing buffer and centrifuged at 20,000 g for 10 min. The supernatant was discarded, and the pellet was resuspended and layered over 36 ml of 27% (vol/vol) Percoll and centrifuged at 20,000 g for 90 min. The lysosomal band in the bottom 1–2 ml was collected and centrifuged at 100,000 g for 1 h, and the turbid layer of lysosomes just above the pellet was collected. After protein quantification, the samples were used for Western blots.

Sarkosyl extraction

Tissues were homogenized in three volumes of cold extraction buffer (25 mM/liter Tris-HCl, pH 7.4, 150 mM/liter NaCl, 1 mM/liter EDTA, 1 mM/liter EGTA, 5 mM/liter sodium pyrophosphate, 10 mM/liter β -glycerophosphate, 30 mM/liter sodium fluoride, 2 mM/liter sodium vanadate, 1 mM/liter phenylmethyl sulfonyl fluoride, and 10 μ g/ml leupeptin, aprotinin, and pepstatin). The homogenates were spun for 15 min at 80,000 g, and the supernatants were used for the analysis of soluble tau. Protein concentrations were determined using the BCA kit (Pierce), and 10 mg of protein was analyzed on 12% SDS-PAGE. To prepare Sarkosyl-insoluble tau, the remaining pellets were homogenized in A68 extraction buffer (10 mM/liter Tris-HCl, pH 7.4, 0.8 M/liter NaCl, 10% sucrose, 1 mM/liter EGTA, 1 mM/liter phenyl-

methyl sulfonyl fluoride, and 10 μ g/ml leupeptin, aprotinin, and pepstatin) and spun at 4,000 g for 20 min. Sarkosyl was then added to 1% to the supernatants, which were left for 1.5 h at room temperature. After a 30-min centrifugation at 80,000 g, the supernatants were discarded, and the pellets were resuspended in 50 mM/liter Tris-HCl, pH 7.4. The samples were analyzed on 12% SDS-PAGE.

AEP activity assay

Tissue homogenates or cell lysates (10 μ g) were incubated in 200 μ l reaction buffer (20 mM citric acid, 60 mM Na_2HPO_4 , 1 mM EDTA, 0.1% CHAPS, and 1 mM DTT, pH 5.5) containing 20 μ M AEP substrate Z-Ala-Ala-Asn-AMC (Bachem). AMC released by substrate cleavage was quantified by measuring at 460 nm in a fluorescence plate reader at 37°C in kinetic mode.

AEP cleavage assay

HEK293 cells were transfected with different plasmids. 48 h after transfection, the cells were lysed in buffer (50 mM sodium citrate, 5 mM DTT, 0.1% CHAPS, 0.5% Triton X-100, 1 mM EDTA, and 60 mM Na_2HPO_4 , pH 5.5) and centrifuged for 15 min at 14,000 g at 4°C. The supernatants were then incubated at 37°C for 0, 5, 10, 15, 30, and 60 min. The samples were then boiled in 1 \times SDS loading buffer and analyzed by immunoblotting.

Immunoprecipitation and Western blot analysis

Cells were washed with ice-cold PBS and lysed in coimmunoprecipitation buffer (50 mM Tris-HCl, pH 7.5, 150 mM NaCl, 1% Nonidet P-40, 5 mM EDTA, 5 mM EGTA, 15 mM MgCl_2 , 60 mM β -glycerophosphate, 0.1 mM sodium orthovanadate, 0.1 mM NaF, 0.1 mM benzamide, 10 μ g/ml aprotinin, 10 μ g/ml leupeptin, and 1 mM PMSF) at 4°C for 2 h with rotation. Immunoprecipitated proteins were separated by SDS-PAGE and then transferred to a nitrocellulose membrane. The membrane was blocked with TBS containing 5% nonfat milk and 0.1% Tween 20 (TBST) at room temperature for 1 h, followed by the incubation with primary antibody at 4°C overnight, and with the secondary antibody at room temperature for 1 h. After washing with TBST, the membrane was developed using the ECL detection system.

IHC

IHC was performed by using the peroxidase protocol. In brief, tissue sections were deparaffinized in xylene, hydrated through descending ethanol, and endogenous peroxidase activity was eliminated by incubation in 3% hydrogen peroxide in methanol for 5 min. After antigen-retrieval in boiling sodium citrate buffer (10 mM), the sections were incubated with primary antibodies for overnight at 4°C. The signal was developed using Histostain-SP kit (Invitrogen). For the double immunofluorescence staining, the sections were incubated overnight at 4°C with a mixture of antibodies. After being washed with TBS, the sections were incubated with a mixture of Alexa Fluor 488- and 568-coupled secondary antibodies (Invitrogen) for detection. Images were acquired through Confocal (Olympus FV1000). The Olympus FV1000 is equipped with four 405-, 488-, 515-, 543-, and 635-nm laser lines and 10 \times 0.4 numerical aperture (NA), 20 \times 0.75 NA, 40 \times 1.3 NA, oil, 60 \times 1.49 NA, oil, 100 \times 1.45 NA, and oil ob-

jectives. Acquisition Software is Olympus Fluoview v4.2. ImageJ was used for the intensity and colocalization analysis.

Gallyas silver staining

Silver staining was performed using the Gallyas method. A semi-quantitative subjective scoring system was developed based on relative numbers of silver-positive cells per section, analyzing four sections per animal. Silver stain scoring was based on the numbers of positive neurons, not intensity, which can vary between sections. After deparaffinization, 5- μ m sections were incubated in 5% periodic acid for 5 min, washed in water, and then placed in alkaline silver iodide solution (containing 1% silver nitrate) for 1 min. The sections were then washed in 0.5% acetic acid for 10 min, placed in developer solution for 15 min, before washing with 0.5% acetic acid, then water. The sections were then treated with 0.1% gold chloride for 5 min before washing in water, and incubation in 1% sodium thiosulphate (hypo) for 5 min, before a final wash.

EM

After deep anesthesia, mice were perfused transcardially with 2% glutaraldehyde and 3% paraformaldehyde in PBS. Hippocampal slices were post-fixed in cold 1% OsO₄ for 1 h. Samples were prepared and examined using standard procedures. Ultrathin sections (90 nm) were stained with uranyl acetate and lead acetate and viewed at 100 kV in a JEOL 200CX electron microscope. Synapses were identified by the presence of synaptic vesicles and post-synaptic densities.

Stereotaxic injection of LV in mouse CA1

Mice were anesthetized with isoflurane, and LV (3 μ l with similar titers $>1 \times 10^9$ IU/ml) were delivered at a rate of 0.3 μ l/min (anteroposterior, -2.2 mm; mediolateral, ± 1.7 mm; dorsoventral, -1.6 mm). Mice were assigned into gender- and age-matched treatment groups using a randomized block design.

Golgi staining

Mouse brains were fixed in 10% formalin for 24 h, and then immersed in 3% potassium bichromate for 3 d in the dark. The solution was changed each day. Then the brains were transferred into 2% silver nitrate solution and incubated for 24 h in the dark. Vibratome sections were cut at 60 μ m, air dried for 10 min, dehydrated through 95% and 100% ethanol, cleared in xylene, and coverslipped.

Electrophysiology

Acute hippocampal transversal slices were prepared from mice injected with LV as previously described (Zhang et al., 2014, 2015). In brief, mice were anaesthetized with isoflurane, decapitated, and their brains were dropped in ice-cold artificial cerebrospinal fluid (a-CSF) containing 124 mM NaCl, 3 mM KCl, 1.25 mM NaH₂PO₄, 6.0 mM MgCl₂, 26 mM NaHCO₃, 2.0 mM CaCl₂, and 10 mM glucose. Hippocampi were dissected and cut into 400- μ m-thick transverse slices with a vibratome. After incubation at room temperature (23–24°C) in a-CSF for 60–90 min, slices were placed in a recording chamber (RC-22C; Warner Instruments) on the stage of an upright microscope (Olympus CX-31) and perfused at a rate of 3 ml/min with a-CSF (containing

1 mM MgCl₂) at 23–24°C. A 0.1 M Ω tungsten monopolar electrode was used to stimulate the Schaffer collaterals. The fEPSPs were recorded in CA1 stratum radiatum by a glass microelectrode filled with a-CSF with a resistance of 3–4 M Ω . The stimulation output (Master-8; AMPI) was controlled by the trigger function of an EPC9 amplifier (HEKA Elektronik). fEPSPs were recorded under current-clamp mode. Data were filtered at 3 kHz and digitized at sampling rates of 20 kHz using Pulse software (HEKA Elektronik). The stimulus intensity (0.1-ms duration, 10–30 μ A) was set to evoke 40% of the maximum fEPSP, and the test pulse was applied at a rate of 0.033 Hz. LTP of fEPSPs was induced by three TBSs (four pulses at 100 Hz, repeated three times with a 200-ms interval). The magnitudes of LTP are expressed as the mean percentage of baseline fEPSP initial slope.

MWM

Mice injected with the various LVs were trained in a round, water-filled tub (52-inch diameter) in an environment rich with extra maze cues as described previously (Zhang et al., 2014). Each subject was given four trials a day for five consecutive days with a 15-min intertrial interval. The maximum trial length was 60 s, and if subjects did not reach the platform in the allotted time, they were manually guided to it. Following the 5 d of task acquisition, a probe trial was presented, during which time the platform was removed, and the percentage of time spent in the quadrant that previously contained the escape platform during task acquisition was measured over 60 s. All trials were analyzed for latency and swim speed by means of MazeScan (Clever Sys, Inc.).

Contextual fear conditioning

The ability to form and retain an association between an aversive experience and environmental cues was tested with a standard fear conditioning paradigm that occurred over a period of 3 d. Mice were placed in the fear conditioning apparatus (width, 7 inches; depth, 7 inches; height, 12 inches; Coulbourn) composed of Plexiglass with a metal shock grid floor and allowed to explore the enclosure for 3 min. Following this habituation period, three conditioned stimulus (CS)–unconditioned stimulus (US) pairings were presented with a 1-min intertrial interval. The CS was composed of a 20-s, 85-dB tone, and US was composed of 2 s of a 0.5-mA foot shock, which was coterminate with each CS presentation. 1 min following the last CS–US presentation, mice were returned to their home cage. On day 2, the mice were presented with a context test, during which subjects were placed in the same chamber used during conditioning on day 1, and the amount of freezing was recorded via a camera and the software provided by Coulbourn. No shocks were given during the context test. On day 3, a tone test was presented, during which time subjects were exposed to the CS in a novel compartment. Initially, animals were allowed to explore the novel context for 2 min. Then the 85-dB tone was presented for 6 min and the amount of freezing behavior was recorded.

Nesting activity

Mice were individually housed and previous nesting material was removed. An intact 3.0-g nestlet was placed within the cages. Approximately 14 h later, following the nocturnal period, untorn nestlet was weighed.

Quantification and statistical analysis

All data are expressed as mean \pm SEM from three or more independent experiments, and the level of significance between two groups was assessed with Student's *t* test. For more than two groups, one-way ANOVA followed by least-significant difference post hoc test was applied. A value of $P < 0.05$ was considered to be statistically significant.

Online supplemental material

Fig. S1, related to Fig. 1, presents additional evidence showing that AEP cleaves SRPK2 in vitro. Fig. S2, related to Fig. 2, presents validation of the specificity of anti-cleaved SRPK2 antibodies. Fig. S3, related to Fig. 2, presents additional information of AEP-cleaved SRPK2 in human 4R-tauopathy brains. Fig. S4, related to Fig. 3, additionally shows that cleavage of SRPK2 by AEP enhances its kinase activity. Fig. S5, related to Fig. 6 and Fig. 7, shows that AEP-truncated SRPK2 in hippocampal CA1 accelerates the synapse loss and exacerbates cognitive impairment in mouse models of tauopathy. Table S1 provides information on reagents and resources of this study.

Acknowledgments

We thank AD Research Center at Emory University for human patients and healthy control samples. The authors are thankful to Dr. Fei Liu for the tau exon 10 mini-gene plasmid and Mr. Duc Duong in the Proteomic Core facility at Emory for analyzing SRPK2 truncates.

This work was supported by grants from National Natural Science Foundation of China (NSFC; no. 81471104), NIH grant AG051538 to K. Ye, and NSFC grants (nos. 81528007 and 31730035) to K. Ye and/or J.-Z. Wang.

The authors declare no competing financial interests.

Author contributions: K. Ye conceived the project, designed the experiments, analyzed the data, and wrote the manuscript. Z.-H. Wang designed and performed most of the experiments. P. Liu and X. Liu prepared primary neurons and assisted with animal experiments. S.-P. Yi and J.-Z. Wang assisted with data analysis and interpretation and critically read the manuscript.

Submitted: 17 March 2018

Revised: 16 August 2018

Accepted: 24 September 2018

References

- Andorfer, C., Y. Kress, M. Espinoza, R. de Silva, K.L. Tucker, Y.A. Barde, K. Duff, and P. Davies. 2003. Hyperphosphorylation and aggregation of tau in mice expressing normal human tau isoforms. *J. Neurochem.* 86:582–590. <https://doi.org/10.1046/j.1471-4159.2003.01879.x>
- Andreadis, A. 2005. Tau gene alternative splicing: expression patterns, regulation and modulation of function in normal brain and neurodegenerative diseases. *Biochim. Biophys. Acta.* 1739:91–103. <https://doi.org/10.1016/j.bbadis.2004.08.010>
- Andreadis, A. 2012. Tau splicing and the intricacies of dementia. *J. Cell. Physiol.* 227:1220–1225. <https://doi.org/10.1002/jcp.22842>
- Bai, B., C.M. Hales, P.C. Chen, Y. Gozal, E.B. Dammer, J.J. Fritz, X. Wang, Q. Xia, D.M. Duong, C. Street, et al. 2013. U1 small nuclear ribonucleoprotein complex and RNA splicing alterations in Alzheimer's disease. *Proc. Natl. Acad. Sci. USA.* 110:16562–16567. <https://doi.org/10.1073/pnas.1310249110>
- Bai, B., P.C. Chen, C.M. Hales, Z. Wu, V. Pagala, A.A. High, A.I. Levey, J.J. Lah, and J. Peng. 2014. Integrated approaches for analyzing U1-70K cleavage in Alzheimer's disease. *J. Proteome Res.* 13:4526–4534. <https://doi.org/10.1021/pr5003593>
- Basurto-Islas, G., I. Grundke-Iqbal, Y.C. Tung, F. Liu, and K. Iqbal. 2013. Activation of asparaginyl endopeptidase leads to Tau hyperphosphorylation in Alzheimer disease. *J. Biol. Chem.* 288:17495–17507. <https://doi.org/10.1074/jbc.M112.446070>
- Bronner, I.F., B.C. ter Meulen, A. Azmani, L.A. Severijnen, R. Willemsen, W. Kamberhorst, R. Ravid, P. Heutink, and J.C. van Swieten. 2005. Hereditary Pick's disease with the G272V tau mutation shows predominant three-repeat tau pathology. *Brain.* 128:2645–2653. <https://doi.org/10.1093/brain/awh591>
- Chan, C.B., and K. Ye. 2013. Serine-arginine protein kinases: new players in neurodegenerative diseases? *Rev. Neurosci.* 24:401–413. <https://doi.org/10.1515/revneuro-2013-0014>
- Chen, C., N. Jin, W. Qian, W. Liu, X. Tan, F. Ding, X. Gu, K. Iqbal, C.X. Gong, J. Zuo, and F. Liu. 2014. Cyclic AMP-dependent protein kinase enhances SC35-promoted Tau exon 10 inclusion. *Mol. Neurobiol.* 49:615–624. <https://doi.org/10.1007/s12035-013-8542-3>
- Connell, J.W., T. Rodriguez-Martin, G.M. Gibb, N.M. Kahn, A.J. Grierson, D.P. Hanger, T. Revesz, P.L. Lantos, B.H. Anderton, and J.-M. Gallo. 2005. Quantitative analysis of tau isoform transcripts in sporadic tauopathies. *Brain Res. Mol. Brain Res.* 137:104–109. <https://doi.org/10.1016/j.molbrainres.2005.02.014>
- Ding, J.H., X.Y. Zhong, J.C. Hagopian, M.M. Cruz, G. Ghosh, J. Feramisco, J.A. Adams, and X.D. Fu. 2006. Regulated cellular partitioning of SR protein-specific kinases in mammalian cells. *Mol. Biol. Cell.* 17:876–885. <https://doi.org/10.1091/mbc.e05-10-0963>
- Ding, S., J. Shi, W. Qian, K. Iqbal, I. Grundke-Iqbal, C.X. Gong, and F. Liu. 2012. Regulation of alternative splicing of tau exon 10 by 9G8 and Dyrk1A. *Neurobiol. Aging.* 33:1389–1399. <https://doi.org/10.1016/j.neurobiolaging.2010.11.021>
- Doran, M., D.G. du Plessis, E.J. Ghadiali, D.M. Mann, S. Pickering-Brown, and A.J. Larner. 2007. Familial early-onset dementia with tau intron 10 + 16 mutation with clinical features similar to those of Alzheimer disease. *Arch. Neurol.* 64:1535–1539. <https://doi.org/10.1001/archneur.64.10.1535>
- Espinoza, M., R. de Silva, D.W. Dickson, and P. Davies. 2008. Differential incorporation of tau isoforms in Alzheimer's disease. *J. Alzheimers Dis.* 14:1–16. <https://doi.org/10.3233/JAD-2008-14101>
- Foster, N.L., K. Wilhelmsen, A.A. Sima, M.Z. Jones, C.J. D'Amato, and S. Gilman. Conference Participants. 1997. Frontotemporal dementia and parkinsonism linked to chromosome 17: a consensus conference. *Ann. Neurol.* 41:706–715. <https://doi.org/10.1002/ana.410410606>
- Ghetti, B., A.L. Oblak, B.F. Boeve, K.A. Johnson, B.C. Dickerson, and M. Goedert. 2015. Invited review: Frontotemporal dementia caused by microtubule-associated protein tau gene (MAPT) mutations: a chameleon for neuropathology and neuroimaging. *Neuropathol. Appl. Neurobiol.* 41:24–46. <https://doi.org/10.1111/nan.12213>
- Giannakouros, T., E. Nikolakaki, I. Mylonis, and E. Georgatsou. 2011. Serine-arginine protein kinases: a small protein kinase family with a large cellular presence. *FEBS J.* 278:570–586. <https://doi.org/10.1111/j.1742-4658.2010.07987.x>
- Goedert, M., and R. Jakes. 2005. Mutations causing neurodegenerative tauopathies. *Biochim. Biophys. Acta.* 1739:240–250. <https://doi.org/10.1016/j.bbadis.2004.08.007>
- Goedert, M., M.G. Spillantini, R. Jakes, D. Rutherford, and R.A. Crowther. 1989. Multiple isoforms of human microtubule-associated protein tau: sequences and localization in neurofibrillary tangles of Alzheimer's disease. *Neuron.* 3:519–526. [https://doi.org/10.1016/0896-6273\(89\)90210-9](https://doi.org/10.1016/0896-6273(89)90210-9)
- Goedert, M., M.G. Spillantini, R.A. Crowther, S.G. Chen, P. Parchi, M. Tabaton, D.J. Lanska, W.R. Markesbery, K.C. Wilhelmsen, D.W. Dickson, et al. 1999. Tau gene mutation in familial progressive subcortical gliosis. *Nat. Med.* 5:454–457. <https://doi.org/10.1038/7454>
- Gu, J., J. Shi, S. Wu, N. Jin, W. Qian, J. Zhou, I.G. Iqbal, K. Iqbal, C.X. Gong, and F. Liu. 2012. Cyclic AMP-dependent protein kinase regulates 9G8-mediated alternative splicing of tau exon 10. *FEBS Lett.* 586:2239–2244. <https://doi.org/10.1016/j.febslet.2012.05.046>
- Gui, J.F., W.S. Lane, and X.D. Fu. 1994. A serine kinase regulates intracellular localization of splicing factors in the cell cycle. *Nature.* 369:678–682. <https://doi.org/10.1038/369678a0>
- Hales, C.M., E.B. Dammer, I. Diner, H. Yi, N.T. Seyfried, M. Gearing, J.D. Glass, T.J. Montine, A.I. Levey, and J.J. Lah. 2014. Aggregates of small nuclear ribonucleic acids (snRNAs) in Alzheimer's disease. *Brain Pathol.* 24:344–351. <https://doi.org/10.1111/bpa.12133>

- Hartmann, A.M., D. Rujescu, T. Giannakouros, E. Nikolakaki, M. Goedert, E.M. Mandelkow, Q.S. Gao, A. Andreadis, and S. Stamm. 2001. Regulation of alternative splicing of human tau exon 10 by phosphorylation of splicing factors. *Mol. Cell. Neurosci.* 18:80–90. <https://doi.org/10.1006/mcne.2001.1000>
- Hauw, J.-J., S.E. Daniel, D. Dickson, D.S. Horoupian, K. Jellinger, P.L. Lantos, A. McKee, M. Tabaton, and I. Litvan. 1994. Preliminary NINDS neuropathologic criteria for Steele-Richardson-Olszewski syndrome (progressive supranuclear palsy). *Neurology.* 44:2015–2019. <https://doi.org/10.1212/WNL.44.11.2015>
- Hong, Y., S.W. Jang, and K. Ye. 2011. The N-terminal fragment from caspase-cleaved serine/arginine protein-specific kinase2 (SRPK2) translocates into the nucleus and promotes apoptosis. *J. Biol. Chem.* 286:777–786. <https://doi.org/10.1074/jbc.M110.193441>
- Hong, Y., C.B. Chan, I.S. Kwon, X. Li, M. Song, H.P. Lee, X. Liu, P. Sompol, P. Jin, H.G. Lee, et al. 2012. SRPK2 phosphorylates tau and mediates the cognitive defects in Alzheimer's disease. *J. Neurosci.* 32:17262–17272. <https://doi.org/10.1523/JNEUROSCI.3300-12.2012>
- Hutton, M., C.L. Lendon, P. Rizzu, M. Baker, S. Froelich, H. Houlden, S. Pickering-Brown, S. Chakraverty, A. Isaacs, A. Grover, et al. 1998. Association of missense and 5'-splice-site mutations in tau with the inherited dementia FTDP-17. *Nature.* 393:702–705. <https://doi.org/10.1038/31508>
- Ingram, E.M., and M.G. Spillantini. 2002. Tau gene mutations: dissecting the pathogenesis of FTDP-17. *Trends Mol. Med.* 8:555–562. [https://doi.org/10.1016/S1471-4914\(02\)02440-1](https://doi.org/10.1016/S1471-4914(02)02440-1)
- Jang, S.W., S.J. Yang, A. Ehlén, S. Dong, H. Khoury, J. Chen, J.L. Persson, and K. Ye. 2008. Serine/arginine protein-specific kinase 2 promotes leukemia cell proliferation by phosphorylating acinus and regulating cyclin A1. *Cancer Res.* 68:4559–4570. <https://doi.org/10.1158/0008-5472.CAN-08-0021>
- Jang, S.W., X. Liu, H. Fu, H. Rees, M. Yepes, A. Levey, and K. Ye. 2009. Interaction of Akt-phosphorylated SRPK2 with 14-3-3 mediates cell cycle and cell death in neurons. *J. Biol. Chem.* 284:24512–24525. <https://doi.org/10.1074/jbc.M109.026237>
- Janssen, J.C., E.K. Warrington, H.R. Morris, P. Lantos, J. Brown, T. Revesz, N. Wood, M.N. Khan, L. Cipolotti, N.C. Fox, and M.N. Rossor. 2002. Clinical features of frontotemporal dementia due to the intronic tau 10(+16) mutation. *Neurology.* 58:1161–1168. <https://doi.org/10.1212/WNL.58.8.1161>
- Koizumi, J., Y. Okamoto, H. Onogi, A. Mayeda, A.R. Krainer, and M. Hagiwara. 1999. The subcellular localization of SF2/ASF is regulated by direct interaction with SR protein kinases (SRPKs). *J. Biol. Chem.* 274:11125–11131. <https://doi.org/10.1074/jbc.274.16.11125>
- Kornblihtt, A.R., I.E. Schor, M. Alló, G. Dujardin, E. Petrillo, and M.J. Muñoz. 2013. Alternative splicing: a pivotal step between eukaryotic transcription and translation. *Nat. Rev. Mol. Cell Biol.* 14:153–165. <https://doi.org/10.1038/nrm3525>
- Kosik, K.S., L.D. Orecchio, S. Bakalis, and R.L. Neve. 1989. Developmentally regulated expression of specific tau sequences. *Neuron.* 2:1389–1397. [https://doi.org/10.1016/0896-6273\(89\)90077-9](https://doi.org/10.1016/0896-6273(89)90077-9)
- Kuroyanagi, N., H. Onogi, T. Wakabayashi, and M. Hagiwara. 1998. Novel SR-protein-specific kinase, SRPK2, disassembles nuclear speckles. *Biochem. Biophys. Res. Commun.* 242:357–364. <https://doi.org/10.1006/bbrc.1997.7913>
- Lacovich, V., S.L. Espindola, M. Alloati, V. Pozo Devoto, L.E. Cromberg, M.E. Čarná, G. Forte, J.M. Gallo, L. Bruno, G.B. Stokin, et al. 2017. Tau Isoforms Imbalance Impairs the Axonal Transport of the Amyloid Precursor Protein in Human Neurons. *J. Neurosci.* 37:58–69. <https://doi.org/10.1523/JNEUROSCI.2305-16.2016>
- Lantos, P.L., N.J. Cairns, M.N. Khan, A. King, T. Revesz, J.C. Janssen, H. Morris, and M.N. Rossor. 2002. Neuropathologic variation in frontotemporal dementia due to the intronic tau 10(+16) mutation. *Neurology.* 58:1169–1175. <https://doi.org/10.1212/WNL.58.8.1169>
- Liu, F., and C.-X. Gong. 2008. Tau exon 10 alternative splicing and tauopathies. *Mol. Neurodegener.* 3:8. <https://doi.org/10.1186/1750-1326-3-8>
- Manley, J.L., and A.R. Krainer. 2010. A rational nomenclature for serine/arginine-rich protein splicing factors (SR proteins). *Genes Dev.* 24:1073–1074. <https://doi.org/10.1101/gad.1934910>
- Murray, M.E., N. Kouri, W.-L. Lin, C.R. Jack Jr., D.W. Dickson, and P. Vemuri. 2014. Clinicopathologic assessment and imaging of tauopathies in neurodegenerative dementias. *Alzheimers Res. Ther.* 6:1. <https://doi.org/10.1186/alzrt231>
- Neumann, M., W. Schulz-Schaeffer, R.A. Crowther, M.J. Smith, M.G. Spillantini, M. Goedert, and H.A. Kretschmar. 2001. Pick's disease associated with the novel Tau gene mutation K369I. *Ann. Neurol.* 50:503–513. <https://doi.org/10.1002/ana.1223>
- Pickering-Brown, S.M., A.M. Richardson, J.S. Snowden, A.M. McDonagh, A. Burns, W. Braude, M. Baker, W.K. Liu, S.H. Yen, J. Hardy, et al. 2002. Inherited frontotemporal dementia in nine British families associated with intronic mutations in the tau gene. *Brain.* 125:732–751. <https://doi.org/10.1093/brain/awf069>
- Qian, W., H. Liang, J. Shi, N. Jin, I. Grundke-Iqbal, K. Iqbal, C.X. Gong, and F. Liu. 2011. Regulation of the alternative splicing of tau exon 10 by SC35 and Dyrk1A. *Nucleic Acids Res.* 39:6161–6171. <https://doi.org/10.1093/nar/gkr195>
- Schoch, K.M., S.L. DeVos, R.L. Miller, S.J. Chun, M. Norrbom, D.F. Wozniak, H.N. Dawson, C.F. Bennett, F. Rigo, and T.M. Miller. 2016. Increased 4R-Tau Induces Pathological Changes in a Human-Tau Mouse Model. *Neuron.* 90:941–947. <https://doi.org/10.1016/j.neuron.2016.04.042>
- Shi, J., T. Zhang, C. Zhou, M.O. Chohan, X. Gu, J. Wegiel, J. Zhou, Y.W. Hwang, K. Iqbal, I. Grundke-Iqbal, et al. 2008. Increased dosage of Dyrk1A alters alternative splicing factor (ASF)-regulated alternative splicing of tau in Down syndrome. *J. Biol. Chem.* 283:28660–28669. <https://doi.org/10.1074/jbc.M802645200>
- Shi, J., W. Qian, X. Yin, K. Iqbal, I. Grundke-Iqbal, X. Gu, F. Ding, C.X. Gong, and F. Liu. 2011. Cyclic AMP-dependent protein kinase regulates the alternative splicing of tau exon 10: a mechanism involved in tau pathology of Alzheimer disease. *J. Biol. Chem.* 286:14639–14648. <https://doi.org/10.1074/jbc.M110.204453>
- Shirahama-Noda, K., A. Yamamoto, K. Sugihara, N. Hashimoto, M. Asano, M. Nishimura, and I. Hara-Nishimura. 2003. Biosynthetic processing of cathepsins and lysosomal degradation are abolished in asparaginyl endopeptidase-deficient mice. *J. Biol. Chem.* 278:33194–33199. <https://doi.org/10.1074/jbc.M302742200>
- Spillantini, M.G., J.R. Murrell, M. Goedert, M.R. Farlow, A. Klug, and B. Ghetti. 1998. Mutation in the tau gene in familial multiple system tauopathy with presenile dementia. *Proc. Natl. Acad. Sci. USA.* 95:7737–7741. <https://doi.org/10.1073/pnas.95.13.7737>
- Umeda, T., T. Yamashita, T. Kimura, K. Ohnishi, H. Takuma, T. Ozeki, A. Takashima, T. Tomiyama, and H. Mori. 2013. Neurodegenerative disorder FTDP-17-related tau intron 10 +16C → T mutation increases tau exon 10 splicing and causes tauopathy in transgenic mice. *Am. J. Pathol.* 183:211–225. <https://doi.org/10.1016/j.ajpath.2013.03.015>
- Wang, Y., and E. Mandelkow. 2016. Tau in physiology and pathology. *Nat. Rev. Neurosci.* 17:5–21. <https://doi.org/10.1038/nrn.2015.1>
- Wang, H.Y., W. Lin, J.A. Dyck, J.M. Yeakley, Z. Songyang, L.C. Cantley, and X.D. Fu. 1998. SRPK2: a differentially expressed SR protein-specific kinase involved in mediating the interaction and localization of pre-mRNA splicing factors in mammalian cells. *J. Cell Biol.* 140:737–750. <https://doi.org/10.1083/jcb.140.4.737>
- Wang, Z.H., P. Liu, X. Liu, F.P. Manfredsson, I.M. Sandoval, S.P. Yu, J.Z. Wang, and K. Ye. 2017. Delta-Secretase Phosphorylation by SRPK2 Enhances Its Enzymatic Activity, Provoking Pathogenesis in Alzheimer's Disease. *Mol. Cell.* 67:812–825.e5. <https://doi.org/10.1016/j.molcel.2017.07.018>
- Yen, S.H., M. Hutton, M. DeTure, L.W. Ko, and P. Nacharaju. 1999. Fibrillogenesis of tau: insights from tau missense mutations in FTDP-17. *Brain Pathol.* 9:695–705. <https://doi.org/10.1111/j.1750-3639.1999.tb00551.x>
- Yoshida, M. 2006. Cellular tau pathology and immunohistochemical study of tau isoforms in sporadic tauopathies. *Neuropathology.* 26:457–470. <https://doi.org/10.1111/j.1440-1789.2006.00743.x>
- Zhang, Z., M. Song, X. Liu, S.S. Kang, I.S. Kwon, D.M. Duong, N.T. Seyfried, W.T. Hu, Z. Liu, J.Z. Wang, et al. 2014. Cleavage of tau by asparagine endopeptidase mediates the neurofibrillary pathology in Alzheimer's disease. *Nat. Med.* 20:1254–1262. <https://doi.org/10.1038/nm.3700>
- Zhang, Z., M. Song, X. Liu, S. Su Kang, D.M. Duong, N.T. Seyfried, X. Cao, L. Cheng, Y.E. Sun, S. Ping Yu, et al. 2015. Delta-secretase cleaves amyloid precursor protein and regulates the pathogenesis in Alzheimer's disease. *Nat. Commun.* 6:8762. <https://doi.org/10.1038/ncomms9762>
- Zhang, Z., M. Xie, and K. Ye. 2016. Asparagine endopeptidase is an innovative therapeutic target for neurodegenerative diseases. *Expert Opin. Ther. Targets.* 20:1237–1245. <https://doi.org/10.1080/14728222.2016.1182990>
- Zhang, Z., S.S. Kang, X. Liu, E.H. Ahn, Z. Zhang, L. He, P.M. Iuvone, D.M. Duong, N.T. Seyfried, M.J. Benskey, et al. 2017a. Asparagine endopeptidase cleaves α-synuclein and mediates pathologic activities in Parkinson's disease. *Nat. Struct. Mol. Biol.* 24:632–642. <https://doi.org/10.1038/nsmb.3433>
- Zhang, Z., O. Obianyo, E. Dall, Y. Du, H. Fu, X. Liu, S.S. Kang, M. Song, S.P. Yu, C. Cabrele, et al. 2017b. Inhibition of delta-secretase improves cognitive functions in mouse models of Alzheimer's disease. *Nat. Commun.* 8:14740. <https://doi.org/10.1038/ncomms14740>
- Zhong, X.-Y., P. Wang, J. Han, M.G. Rosenfeld, and X.-D. Fu. 2009. SR proteins in vertical integration of gene expression from transcription to RNA processing to translation. *Mol. Cell.* 35:1–10. <https://doi.org/10.1016/j.molcel.2009.06.016>